2012

Fluid-phase velocity fluctuations in gas-solid flows

Mohammad Mehrabadi
Iowa State University

Fluid-phase velocity fluctuations in gas-solid flows

by

Mohammad Mehrabadi

A thesis submitted to the graduate faculty

in partial fulfillment of the requirements for the degree of

MASTER OF SCIENCE

Major: Mechanical Engineering

Program of Study Committee:

Shankar Subramaniam, Major Professor

Terry Meyer

Zhi Jian Wang

Iowa State University

Ames, Iowa

2012

TABLE OF CONTENTS

LIST OF TABLES

LIST OF FIGURES

ACKNOWLEDGEMENTS

I would like to take this opportunity to express my sincere appreciation to those who helped me complete my research, particularly my adviser, Professor Shankar Subramaniam who granted me the opportunity to work with his research group under his supervision. I would also like to express my deepest gratitude to Professor Subramaniam for patiently guiding and helping me through difficult periods of frustration. Over the past few years, I have been fortunate to work with Professor Subramaniam and learn independent research methods, as well as to collaborate with fellow researchers. I would also like to thank my POS committee members, Dr. Terry Meyer and Dr. Zhi Jian Wang, for their support and time. I was also fortunate to have wonderful lab-mates who helped me considerably during my study at Iowa State University of Science and Technology, by supporting to my research through useful discussions. Last but not least, I extend my appreciation to my family who considered education a high priority and encouraged me during the difficult days of academic life.

This work was supported by a Department of Energy grant DE-FC26-07NT43098 through the National Energy Technology Laboratory (NETL).

ABSTRACT

Fluid-phase velocity fluctuations in fixed beds and freely evolving suspensions are quantified using particle-resolved direct numerical simulation (PR-DNS). The flow regime corresponds to homogeneous gas-solid systems typically encountered in fluidized beds, with high solid to fluid density ratios and particle diameters being greater than dissipative length scales. The contribution of turbulent and pseudo-turbulent fluctuations to the level of fluid-phase velocity fluctuations is quantified in flow past fixed particle assemblies. The simulations are then extended to freely evolving suspensions with elastic and inelastic collisions. For the parameter ranges considered here (volume fraction 0.1 and 0.2, particle to fluid density ratio 100 and 1000, coefficient of restitution in the range 0.7–1.0), the level of gas-phase velocity fluctuations in freely evolving suspensions differs by only 10% from the value for a fixed bed at the same solid volume fraction ϕ and mean slip Reynolds number Re_m. Quantification of the Reynolds stress indicates that the second moments of the gas-phase velocity fluctuations are anisotropic, corresponding to unidirectional axisymmetric velocity fluctuations. The anisotropy increases with Re_m to a maximum in the range $10 \leq Re_m \leq 40$, and then decreases. In addition, the anisotropy decreases with increasing solid volume fraction for all cases considered in this study. The Reynolds stress is decomposed into isotropic and deviatoric parts, and their dependence on ϕ and Re_m is quantified and explained.

CHAPTER 1. INTRODUCTION

1.1 Background

Multiphase flow is a system in which several phases such as solid, liquid and gas coexist and interact with each other. Multiphase flows are very common in nature. Motion of raindrops and snowflakes in air, sand storms, volcanic eruptions, and the sedimentation process in rivers are examples of natural occurrences of multiphase flows. These flows are also very common in industrial applications. For instance, in an internal combustion engine, fuel is injected into the combustion chamber and the quality of fuel–air mixture determines the efficiency of the combustion process. In fluidized bed combustors, solid fuel particles are suspended by upward blowing jets of air during the combustion process, providing an effective chemical reaction. In fluid catalytic cracking process, a fluidized powdered catalyst converts the high-molecular weight hydrocarbons of crude oil into gasoline, olefin, and other products (Speight, 2006). A better understanding of the physical phenomena in multiphase flows will help current applications become more efficient. The scope of this study is limited to two-phase flows consisting of solid particles interacting with a gas phase.

In industrial applications of gas-solid flows, particle to fluid density ratio $\rho^{(f)}/\rho^{(f)}$ is of the order of 1000 and particle diameter d_p ranges from 50 to 500μm. In these flows, the particles are usually larger than the dissipative length scale η. The interaction of large particles with carrier flow generates pseudo-turbulent gas-phase velocity fluctuations due to the mean slip velocity (Tenneti et al., 2012). The mean slip velocity is an important parameter because it strongly influences both the asymmetric pressure distribution around particles and the formation of boundary layers on particle surfaces. The asymmetry of pressure is a key mechanism in the formation of wake structures behind the spheres, which are then convected along the mean

slip velocity and contribute to gas-phase velocity fluctuations. The mean slip velocity also generates large velocity gradients in the gap between particles. These velocity gradients modify the dissipation of gas-phase velocity fluctuations, which are no longer characterized by the Kolmogorov scales, unlike the case of single-phase turbulence. These mechanisms determine the level of gas-phase velocity fluctuations in particle-laden flows.

There are several studies in which particles are smaller than the dissipative length scale (Squires and Eaton, 1990; Elghobashi and Truesdell, 1993; Boivin et al., 1998; Sundaram and Collins, 1999). The influence of these small particles, called *point–particles*, on the gas phase depends on the mass loading α. Mass loading is defined as ratio of the total mass of the solid phase to the total mass of the gas phase. In systems with low mass loading ($\alpha \ll 1$), particles do not influence the carrier flow structures; they follow the gas-phase motions. Therefore, a one-way coupling is valid, and the hydrodynamic forces on a particle are usually modeled as a function of the particle Reynolds number. In systems with high mass loading ($\alpha > 1$), the interphase momentum transfer term is significant, and the influence of particles on the gas-phase cannot be ignored. Thus, a two-way coupling is valid, and the interphase momentum transfer term is modeled as a function of flow parameters. Although turbulence modulation has been addressed for point–particles, it has not been comprehensively studied for large particles that modify the flow motions through the formation of boundary layer at particle surface, as well as the wake structures behind particles. The level of gas-phase velocity fluctuations $k^{(f)}$ consists of both carrier flow turbulence, and pseudo-turbulent gas-phase velocity fluctuations resulting from the presence of particles. From a modeling viewpoint, it is essential to distinguish the level of these gas-phase velocity fluctuations and their contributions to $k^{(f)}$.

Experimental investigations of gas-solid flows provide solid information about characteristics of gas-solid flows. Moran and Glicksman (2003) observed that the presence of particles results in substantial enhancement of upstream turbulence intensity as it flows through a fluidized bed compared to gas-phase velocity fluctuations in the absence of particles. The hot wire anemometer technique used by Moran and Glicksman (2003) cannot distinguish the directional components of the velocity fluctuations. Furthermore, it is an intrusive measurement technique, as is the specially designed pitot probe used by Doig and Roper (1967). On the other hand,

non-intrusive methods of laser Doppler anemometry (LDA) (Lee and Durst, 1982; Rogers and Eaton, 1991; Sato et al., 1996), and particle image velocimetry (PIV) (Oakley et al., 1997; Kiger and Pan, 2000) are limited to very dilute systems due to the difficulties with optical access in denser gas-solid systems.

An alternative approach to investigate gas-phase velocity fluctuations in gas-solid flows is to use particle-resolved direct numerical simulation (PR-DNS) that provides detailed spatial and temporal information of the flow field. For gas-solid flows with particle diameters greater than the dissipative length scale, PR-DNS is necessary to resolve all the scales of the carrier flow turbulence and the flow scales introduced by the presence of particles. PR-DNS has been used to study the interaction of decaying isotropic turbulence with a single particle (Bagchi and Balachandar, 2004; Burton and Eaton, 2005) or a collection of particles (Zhang and Prosperetti, 2005), particle-laden turbulent channel flow (Uhlmann, 2008), gas-solid flows with upstream turbulence (Xu and Subramaniam, 2010), and statistically homogeneous pseudo-turbulent gas-solid flows with a mean slip velocity (Tenneti et al., 2012).

Although PR-DNS is an appropriate tool to study gas-solid flows of large particles, it is prohibitively expensive for device-scale calculations. Computational fluid dynamics (CFD) is however the most appropriate tool for device-scale calculations of gas-solid flows that solve averaged conservation equations of mass, momentum and energy for each phase. The averaging process leads to the appearance of unclosed terms such as interphase momentum transfer and correlations of sub-grid velocity fluctuations. The applicability of CFD strongly depends on the accuracy of models for unclosed terms in predicting all the mechanical interactions associated with these terms. These interactions are outlined by Sinclair and Jackson (1989) as:

1. The interaction between the mean velocity of gas phase and the mean velocity of solid phase

2. The interaction between the mean and fluctuating velocities of the gas phase

3. The interaction between the mean and fluctuating velocities of the solid phase

4. The interaction between particles and turbulent motions of the gas phase

There have been several studies focusing on how to incorporate these interactions into hydrodynamics models. In early attempts, gas-phase velocity fluctuations were usually neglected and the main focus was on the first and third interactions (Sinclair and Jackson, 1989; Ding and Gidaspow, 1990; Pita and Sundaresan, 1993) that contribute to the granular temperature. The neglect of gas-phase velocity fluctuations resulted in the uncertainty in the predictive capability and limited ability of early models. These shortcomings, and experimental evidence supporting the importance of fluid-phase velocity fluctuations resulted in the emergence of a new class of models in which the effects of fluid-phase velocity fluctuations were also considered. Louge et al. (1991) and Bolio et al. (1995) were the first to include the effect of gas-phase velocity fluctuations in modeling by means of one-equation and two-equation models for dilute systems of large particles. Subsequently, more sophisticated models such as the four-equation k-ε model of Simonin (1996) were proposed, and valid for a wide range of volume fractions and Reynolds numbers. These models are primarily based on the eddy viscosity hypothesis requiring transport equations for $k^{(f)}$ and dissipation rate of gas-phase velocity fluctuations $\varepsilon^{(f)}$. Thus, single-phase k-ε turbulence models were modified for gas-solid flow applications. However, their validity for dense suspensions with large particles has not been tested. Nevertheless, PR-DNS of gas-solid flows play a key role in understanding the physics governing particulate flows. These findings can be used to propose accurate models capturing the characteristics of gas-solid suspensions. Accordingly, Tenneti et al. (2012) proposed a model for the level of velocity fluctuations in gas-solid flows from PR-DNS over a wide range of Reynolds numbers and solid volume fractions, as well as an eddy viscosity model.

Recent PR-DNS of Xu and Subramaniam (2010), Uhlmann (2008), and Tenneti et al. (2012) indicate that the gas-phase Reynolds stress is strongly anisotropic, playing an important role in anisotropic heat and mass transfer, even in statistically homogeneous suspensions. Level of $k^{(f)}$ as a scalar quantity cannot represent the distribution of fluctuating energy among the Reynolds stresses. Thus, the importance of anisotropy motivates us to quantify the anisotropy in gas-solid flows from our PR-DNS data. This information in conjugation with the proposed model for $k^{(f)}$ can be used to develop a model for gas-phase Reynolds stress.

1.2 Research objectives and approaches

This study addresses the following questions:

1. What are the contributions of turbulent and pseudo-turbulent gas-phase velocity fluctuations to the steady value of $k^{(f)}$ in fluidized beds?

2. How are gas-phase velocity fluctuations affected in freely evolving suspensions of heavy particles?

3. How does the anisotropy of gas-phase Reynolds stress depend on flow parameters?

To answer these questions, we perform PR-DNS of homogeneous gas-solid systems with a finite mean slip velocity in fixed particle assemblies and freely evolving suspensions. The fixed particle assembly simulations are used to determine the relative contribution of turbulent and pseudo-turbulent gas-phase velocity fluctuations to the steady level of $k^{(f)}$. In these simulations the particles are held stationary and a steady flow is established by imposing a mean pressure gradient that corresponds to the desired flow rate. Use of the fixed bed simulation methodology for freely evolving gas-solid flows is justified if the configuration of the particles changes very slowly compared to the time it takes to attain mean momentum balance (Xu and Subramaniam, 2010; Tenneti et al., 2012). However, a direct comparison between fixed and freely evolving suspensions at the same solid volume fraction and Reynolds number has apparently not been reported.

In real particle-laden flows, particles move and collide freely. Numerical simulations of freely evolving suspensions have been performed elsewhere (Yin and Koch, 2007) to study the sedimentation of particles under gravity in the presence of fluid. In these studies the steady mean flow Reynolds number attains a unique value that depends on problem parameters (gas and particle densities, solid volume fraction, gravitational acceleration, etc.). Therefore, in sedimenting suspensions it is not possible to simulate arbitrary Reynolds numbers. However, simulation of freely evolving suspensions in an accelerating frame of reference (Tenneti et al., 2010) enables us to simulate suspensions at arbitrary Reynolds numbers while maintaining other parameters at fixed values. The results are then compared over a wide range of problem

parameters with data from fixed particle assemblies to gain insight into the effect of freely moving particles on gas-phase velocity fluctuations. In addition, we verify the validity of the fixed bed approximation to freely evolving suspensions of high Stokes number particles.

1.3 Report outline

Chapter 2 provides background information about governing equations and the numerical approach. Chapter 3 addresses the research objectives and results, followed by chapter 4 where the main findings are summarized and possible extensions are discussed.

CHAPTER 2. DIRECT NUMERICAL SIMULATION OF GAS–SOLID FLOWS WITH PUReIBM

In this chapter, the formulation of Particle-Resolved Uncontaminated-fluid Reconcilable Immersed Boundary Method (PUReIBM) is introduced. The method is a legacy of Yusof (1996) which was used to simulate the interaction of a single particle with a turbulent flow. It was then developed by Tenneti et al. (2010) to simulate homogeneous gas-solid suspensions with random distribution of particles for both fixed beds and freely evolving suspensions.

2.1 Introduction

Although gas-slid flows have been studied for several decades, design of devices utilizing gas-solid suspensions, such as circulating fluidized beds and coal gasifiers, is still a challenge in industrial applications. Recently, computational fluid dynamics (CFD) has played a key role in such device-scale designs due to the increasing power of computational resources. CFD involves solving averaged conservation equations of mass, momentum and energy for both carrier and dispersed phases. These equations include unclosed interphase transfer terms and sub-grid velocity fluctuation correlations. In modeling, the focus is to relate the unclosed terms to averaged flow quantities. PR-DNS of gas-solid suspensions in canonical flows is the best approach to developing accurate models for unclosed terms (Balachandar and Eaton, 2010) in two-fluid theory. Accordingly, several PR-DNS methods have been developed by various research groups. In the current study, we use PUReIBM based on the immersed boundary method.

2.2 Numerical method

PUReIBM is a robust and highly accurate method for PR-DNS of gas-solid flows. The method is clearly described elsewhere (Garg, 2009; Tenneti et al., 2010). However, for the sake of completeness the method is summarized here.

One of the advantages of PUReIBM over other PR-DNS methods is its flexibility in simulating freely evolving suspensions with arbitrary physical parameters. In numerical investigations of freely evolving suspensions, the sedimentation of particles have usually been studied under the influence of gravity, which leads to a balance between the drag force and the weight of particles (Yin and Koch, 2007). In these simulations, the Reynolds number reaches a unique value dependant upon physical parameters such as fluid and particle densities, and gravitational acceleration. The formulation of PUReIBM in an accelerating frame of reference enables us to simulate arbitrary mean slip Reynolds numbers, while keeping other parameters constant. This feature lets us study the effect of each parameter on a freely evolving gas-solid suspension. In PUReIBM a mean pressure gradient is established along the flow direction to balance the drag force exerted on particles, and also supply the required body force to maintain desired mean slip velocity. Since hydrodynamic forces from the fluid phase cause particles to experience a mean acceleration, the mean pressure gradient should subsequently increase to maintain a constant mean slip velocity between the two phases. Therefore, a steady state solution in the laboratory frame is non-existent. The continuous growth of characteristic velocities in the laboratory frame decreases the time stepping of the numerical method due to the Courant number criterion. Thus, the simulation of freely evolving suspensions in the laboratory frame would be prohibitively restricted to short periods of evolution time.

In PUReIBM, the velocity, pressure, and tensor fields are continuous. However, particle presence is represented by implementing the no-slip and no-penetration boundary conditions at the surface of particles. The strategy is similar to conventional CFD approaches where the boundaries are satisfied by considering a ghost cell beyond the physical domain (Patankar 1980), and reversing the flow so the relative velocity between the two faces becomes zero at the interface. In PUReIBM, the required immersed boundary forcing is only effective to the com-

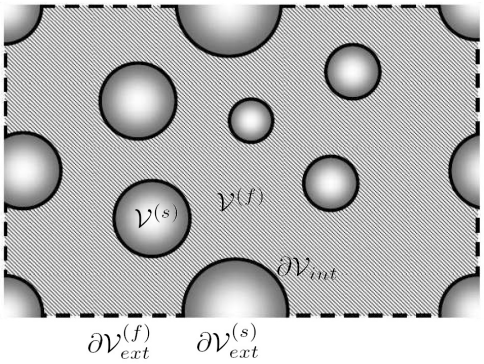

Figure 2.1 Schematic of the computational with multiple particles in PUReIBM. The volumes of fluid and solid phases are denoted by $\mathcal{V}^{(f)}$ and $\mathcal{V}^{(p)}$, respectively. The boundary surfaces of the fluid and solid phases are denoted by $\partial\mathcal{V}_{ext}^{(f)}$ and $\partial\mathcal{V}_{ext}^{(p)}$, respectively. The fluid and solid interface in computational domain is indicated by $\partial\mathcal{V}_{int}$.

putational nodes inside the particles. Thus, the fluid-phase solution remains uncontaminated compared to conventional immersed boundary methods (Peskin, 2002). This approach enables us to directly compute the drag force by integrating the stress tensor over the particle surface.

In PUReIBM, an Eulerian description is used for the carrier phase and a Lagrangian description is used for the dispersed phase. Governing equations are solved over a Cartesian grid, providing simplicity and generality of the numerical method, compared to body fitted grid methods encompassing huge computational remeshing loads. The conservation equations of mass and momentum in the laboratory and accelerating frames are related to each other. If the laboratory frame and non-inertial frame are denoted by E and $\overline{E}$ respectively, the velocity, position and time between these two frames are transformed as

$$\begin{aligned} \overline{\mathbf{u}} &= \mathbf{u} - \mathbf{V}_f, \\ \overline{\mathbf{x}} &= \mathbf{x} - \int_0^t \mathbf{V}_f(t')dt', \\ \bar{t} &= t, \end{aligned} \tag{2.1}$$

where $\mathbf{V}_f$ is the accelerating frame velocity, $\mathbf{x}$, t, and $\mathbf{u}$ are position, time and velocity in the laboratory frame, and those with a bar corresponding to quantities in the accelerating frame. The governing equations of the fluid phase are conservation equations of mass and momentum, solved for both carrier and dispersed phases with periodic boundary conditions. Fig. 2.1 shows a schematic periodic configuration of the simulation setup. Continuity and momentum equations

in the accelerating frame $\overline{E}$ are given as (Pope, 2000)

$$\nabla \cdot \overline{\mathbf{u}} = 0, \tag{2.2}$$

and

$$\frac{\partial \overline{\mathbf{u}}}{\partial \overline{t}} + \overline{\mathbf{S}} = -\frac{1}{\rho^{(f)}}\overline{\mathbf{g}} + \nu^{(f)}\nabla^2\overline{\mathbf{u}} + \frac{1}{\rho^{(f)}}\overline{\mathbf{f}} - \mathbf{A}_f, \tag{2.3}$$

respectively, where $\overline{\mathbf{u}}$ is the instantaneous velocity, $\overline{\mathbf{S}} = \nabla \cdot (\overline{\mathbf{u}}\overline{\mathbf{u}})$ is the convective term in conservative form, $\overline{\mathbf{g}}$ is the pressure gradient, $\overline{\mathbf{f}}$ is the immersed boundary forcing in response to the presence of particles satisfying the boundary condition at the particle-fluid interface, and $\mathbf{A}_f$ is the frame acceleration.

The instantaneous quantities can be divided into into mean and fluctuating components. Thus, for a given quantity $Q(\mathbf{x}, t)$, we have

$$Q(\mathbf{x}, t) = \langle Q(t) \rangle_{\mathcal{V}} + Q'(\mathbf{x}, t), \tag{2.4}$$

with Q' being the fluctuating component, and $\langle . \rangle$ denoting the ensemble average. In statistically homogeneous fields, ensemble average is equivalent to the volumetric average, that is

$$\langle Q(t) \rangle_{\mathcal{V}} = \frac{1}{V}\int_{\mathcal{V}} Q(\mathbf{x}, t) dV. \tag{2.5}$$

The mean conservation equations of mass and momentum can be obtained by using the above averaging process in Eqs. 2.2 and 2.3, and integrating them over the computational volume. The resulting equations are

$$\nabla \cdot \langle \overline{\mathbf{u}} \rangle_{\mathcal{V}} = 0, \tag{2.6}$$

and

$$\frac{\partial \langle \overline{\mathbf{u}} \rangle_{\mathcal{V}}}{\partial \overline{t}} = -\frac{1}{\rho^{(f)}} \langle \overline{\mathbf{g}} \rangle_{\mathcal{V}} + \frac{1}{\rho^{(f)}} \langle \overline{\mathbf{f}} \rangle_{\mathcal{V}} - \mathbf{A}_f, \tag{2.7}$$

for the mean conservation of mass and momentum, respectively. Subtracting the above equations from Eqs. 2.2 and 2.3 results in the fluctuating conservation equations of mass and momentum, given as

$$\nabla \cdot \overline{\mathbf{u}}' = 0 \tag{2.8}$$

and

$$\frac{\partial \overline{\mathbf{u}}'}{\partial \overline{t}} + \overline{\mathbf{S}} = -\frac{1}{\rho^{(f)}}\overline{\mathbf{g}}' + \nu^{(f)}\nabla^2\overline{\mathbf{u}}' + \frac{1}{\rho^{(f)}}\overline{\mathbf{f}}', \tag{2.9}$$

respectively. As mentioned earlier, the system's driving force is the mean pressure gradient balancing the drag force exerted on particles, and maintaining a constant mean slip velocity between the two phases. To obtain an expression for the evolution of mean pressure gradient, the phasic mean momentum equation of the fluid phase is determined by integrating Eq. 2.3 over the fluid phase, providing

$$\frac{d}{d\overline{t}}\left\langle \overline{\mathbf{u}}^{(f)} \right\rangle = -\frac{1}{\rho^{(f)}} \left\langle \overline{\mathbf{g}} \right\rangle_{\mathcal{V}} - \frac{1}{\rho^{(f)} V^{(f)}} \oint_{\partial \mathcal{V}^{(p)}} \left(-\psi' \boldsymbol{\delta} + \mu^{(f)} \nabla \overline{\mathbf{u}} \right) \cdot \mathbf{n}^{(p)} dA - \mathbf{A}_f, \tag{2.10}$$

where ψ' is the fluctuating pressure, $\boldsymbol{\delta}$ is the Kronecker delta, $V^{(f)}$ is the fluid volume, $\partial \mathcal{V}^{(p)}$ is the solid surface boundaries, and $\mathbf{n}^{(p)}$ is the normal vector at the particle surface pointing outward toward the fluid phase. Rearrangement of the above equation leads to an expression for the mean pressure gradient as

$$-\frac{1}{\rho^{(f)}} \left\langle \overline{\mathbf{g}} \right\rangle_{\mathcal{V}} = \frac{d}{d\overline{t}}\left\langle \overline{\mathbf{u}}^{(f)} \right\rangle + \frac{1}{\rho^{(f)} V^{(f)}} \oint_{\partial \mathcal{V}^{(p)}} \left(-\psi' \boldsymbol{\delta} + \mu^{(f)} \nabla \overline{\mathbf{u}} \right) \cdot \mathbf{n}^{(p)} dA + \mathbf{A}_f. \tag{2.11}$$

The mean pressure gradient cannot be determined since the frame acceleration is not specified. Thus, one would need to deduce the phasic mean momentum equation of the solid phase to obtain an expression for this quantity. Accordingly, the governing equation of motion for particles in the laboratory frame (with Lagrangian description) is

$$m \frac{d\mathbf{V}^{(m)}}{dt} = \oint_{\partial \mathcal{V}^{(m)}(t)} (-\psi \boldsymbol{\delta} + \mu_f \nabla \mathbf{u}) \cdot \mathbf{n}^{(m)} dA \tag{2.12}$$

where m is the mass of each particle, ψ is the pressure, and the superscript (m) denotes the m^{th} sphere in the particle assembly. By transforming the velocity of the m^{th} particle into the accelerating frame by $\overline{\mathbf{V}}^{(m)}(t) = \mathbf{V}^{(m)}(t) - \mathbf{V}_f(t)$, and using $\left\langle \overline{\mathbf{u}}^{(p)} \right\rangle = (1/N_p) \sum_{m=1}^{N_p} \overline{\mathbf{V}}^{(m)}$ as an averaging operator, the phasic mean momentum equation of the solid phase is obtained as

$$\frac{d}{d\overline{t}}\left\langle \overline{\mathbf{u}}^{(p)} \right\rangle = -\frac{1}{\rho^{(f)}} \left\langle \overline{\mathbf{g}} \right\rangle_{\mathcal{V}} - \frac{1}{\rho^{(p)} V^{(p)}} \oint_{\partial \mathcal{V}^{(p)}} \left(-\psi' \boldsymbol{\delta} + \mu^{(f)} \nabla \overline{\mathbf{u}} \right) \cdot \mathbf{n}^{(p)} dA - \mathbf{A}_f, \tag{2.13}$$

where $\rho^{(p)}$ is the particle density and $V^{(p)}$ is the solid-phase volume. Rearrangement of the above equation leads to another mean pressure gradient expression as

$$-\frac{1}{\rho^{(p)}} \left\langle \overline{\mathbf{g}} \right\rangle_{\mathcal{V}} = \frac{d}{d\overline{t}}\left\langle \overline{\mathbf{u}}^{(p)} \right\rangle + \frac{1}{\rho^{(p)} V^{(p)}} \oint_{\partial \mathcal{V}^{(p)}} \left(-\psi' \boldsymbol{\delta} + \mu^{(f)} \nabla \overline{\mathbf{u}} \right) \cdot \mathbf{n}^{(p)} dA + \mathbf{A}_f. \tag{2.14}$$

In Eqs. 2.11 and 2.14, the integral term is the total drag force acting on particles (denoted as $\overline{\mathbf{F}}_D$ from hereon) reconcilable to the average interphase momentum transfer $\left\langle \tau'_{ji} n_j^{(f)} \delta\left(\mathbf{x}-\mathbf{x}^{(I)}\right)\right\rangle$ in the two-fluid theory (Drew, 1983). Eliminating the frame acceleration between these two equations gives a general closed expression for the mean pressure gradient

$$\left(\frac{1}{\rho^{(f)}}-\frac{1}{\rho^{(p)}}\right)\langle\overline{\mathbf{g}}\rangle_{\mathcal{V}} = \frac{d}{d\bar{t}}\left\langle\overline{\mathbf{u}}^{(p)}\right\rangle - \frac{d}{d\bar{t}}\left\langle\overline{\mathbf{u}}^{(f)}\right\rangle - \frac{\overline{\mathbf{F}}_D}{\mathcal{V}}\left\{\frac{1}{\phi\rho^{(p)}}+\frac{1}{(1-\phi)\rho^{(f)}}\right\}. \tag{2.15}$$

Since the mean solid velocity is zero in the accelerating frame of reference, the solid-phase unsteady term in this equation is zero. Additionally, the fluid-phase unsteady term at each time step is estimated by a finite difference expression, enabling the mean fluid velocity to attain a desired value $\left\langle\overline{\mathbf{u}}^{(f)}\right\rangle^d$, determined by the Reynolds number. Hence, the unsteady term in Eq. 2.15 is discretized as

$$\frac{d}{d\bar{t}}\left\langle\overline{\mathbf{u}}^{(f)}\right\rangle^{k+1} = \frac{\left\langle\overline{\mathbf{u}}^{(f)}\right\rangle^d - \left\langle\overline{\mathbf{u}}^{(f)}\right\rangle^k}{\Delta\bar{t}}, \tag{2.16}$$

where superscripts k and $k+1$ denote the k^{th} and $k+1^{th}$ time steps, respectively. Therefore, the mean pressure gradient is estimated as

$$\left(\frac{1}{\rho^{(f)}}-\frac{1}{\rho^{(p)}}\right)\langle\overline{\mathbf{g}}\rangle_{\mathcal{V}}^{k+1} = -\frac{\left\langle\overline{\mathbf{u}}^{(f)}\right\rangle^d - \left\langle\overline{\mathbf{u}}^{(f)}\right\rangle^k}{\Delta\bar{t}} - \frac{\overline{\mathbf{F}}_D^k}{\mathcal{V}}\left\{\frac{1}{\phi\rho^{(p)}}+\frac{1}{(1-\phi)\rho^{(f)}}\right\}, \tag{2.17}$$

Accordingly, by knowing the mean pressure gradient, the frame acceleration is determined from Eq. 2.14, that is

$$\mathbf{A}_f^{k+1} = \frac{1}{\rho^{(p)}}\left(-\langle\overline{\mathbf{g}}\rangle_{\mathcal{V}}^{k+1} + \frac{\overline{F}_{D,i}^k}{\phi\mathcal{V}}\right). \tag{2.18}$$

Although these formulations are derived for freely evolving suspensions, the fixed particle assembly equations are recovered (Garg et al., 2011) in the limiting case of massive particles ($1/\rho^{(p)} \to 0$).

In PUReIBM, due to the periodicity of the fluctuating fields, a pseudo-spectral method is used with Crank-Nicolson scheme for the viscous terms and an Adams-Bashforth scheme for the convective terms. A fractional time-stepping method based on Kim and Moin's approach (Kim and Moin, 1985) is used to advance the fluctuating velocities in time. Garg et al. (2011) and Tenneti et al. (2011) have shown that PUReIBM is numerically convergent and accurate in describing the drag force for DNS of gas-solid flows. The method is validated through

a comprehensive set of tests: (i) flow past an isolated sphere (ii) Stokes flow past SC and FCC arrangements (ranging from dilute to close-packed limit) compared with the boundary-integral method of Zick and Homsy (1982), (iii) Stokes flow past random arrays of monodisperse spheres compared with LBM simulations of van der Hoef et al. (2005), (iv) moderate to high Reynolds numbers ($Re_m = 300$) in SC and FCC arrangements compared with LBM simulations of Hill et al. (2001), and (v) high Reynolds number flow past random arrays of monodisperse spheres with ANSYS–FLUENT CFD package. It is also shown that PUReIBM is numerically convergent for gas-phase velocity fluctuations (Tenneti et al., 2012), and the dissipation of gas-phase fluctuating velocities (see Appendix B).

CHAPTER 3. GAS–PHASE VELOCITY FLUCTUATIONS IN STATISTICALLY HOMOGENEOUS FIXED PARTICLE BEDS AND FREELY EVOLVING SUSPENSIONS USING PARTICLE–RESOLVED DIRECT NUMERICAL SIMULATION

This chapter is a manuscript submitted to International Journal of Multiphase Flow, titled "Gas-phase velocity fluctuations in statistically homogeneous fixed particle beds and freely evolving suspensions using particle-resolved direct numerical simulation", authored by Mohammad Mehrabadi, Sudheer Tenneti and Shankar Subramaniam.

Abstract

Gas-phase velocity fluctuations in fixed particle beds and freely evolving suspensions are quantified using particle-resolved direct numerical simulation (PR-DNS). The flow regime corresponds to homogeneous gas-solid systems typically encountered in fluidized bed risers, with high solid to gas density ratio and particle diameter being greater than the dissipative length scales. The contribution of turbulent and pseudo-turbulent fluctuations to the level of gas-phase velocity fluctuations is quantified in flow past fixed particle assemblies. The simulations are then extended to freely evolving suspensions with elastic and inelastic collisions. It is found that for the parameter values considered here (solid volume fraction 0.1 and 0.2, particle to gas density ratio 100 and 1000, and coefficient of restitution in the range 0.7-1.0) the level of gas-phase velocity fluctuations in freely evolving suspensions differs by only 10% from the value for a fixed bed at the same solid volume fraction ϕ and mean slip Reynolds number Re_m. Quantification of the Reynolds stress indicates that the second moments of the gas-phase velocity fluctuations are anisotropic, corresponding to unidirectional axisymmetric fluctuations.

The anisotropy increases with Re_m to a maximum that occurs in the range $10 \leq Re_m \leq 40$, and then decreases. In addition, the anisotropy decreases with increasing solid volume fraction for all cases considered in this study. The Reynolds stress is decomposed into isotropic and deviatoric parts, and their dependence on ϕ and Re_m is quantified and explained.

3.1 Introduction

Gas-solid flows are commonly found in industrial applications such as fluidized-bed combustion, fluid catalytic cracking, coal gasification processes, and biomass energy generation (Fan et al., 2004). The interaction of gas-phase velocity fluctuations with solid particles results in flow structures, such as the core annular structure in circulating fluidized beds. In modeling of dilute suspensions based on averaged equations, Louge et al. (1991) and Bolio et al. (1995) have identified both gas-phase velocity fluctuations and particle-particle interaction as key mechanisms that must be accurately modeled in order to capture this phenomenon. In addition, gas-phase velocity fluctuations enhance the heat transfer and mixing of chemical species inside the fluidized bed. This motivates the current study that is focused on understanding the origin and mechanisms responsible for the generation of gas-phase velocity fluctuations in fluidized beds is essential.

In industrial applications of particulate flows, particles are inertial ($\rho^{(p)}/\rho^{(f)} \sim 1000$) with diameter d_p ranging from 50 to $500\mu m$. In these flows, the particles are usually larger than the length scale of dissipative flow motions η. The interaction of large particles with carrier flow generates pseudo-turbulent gas-phase velocity fluctuations due to the mean slip velocity (Tenneti et al., 2012). The mean slip velocity is an important parameter because it strongly influences both the asymmetric pressure distribution around particles and the formation of boundary layers on particle surfaces. The pressure asymmetry results in the formation of wake structures behind the spheres, which are convected downstream by the carrier flow and contribute to gas-phase velocity fluctuations. The mean slip velocity also generates large velocity gradients in particle interstices. These local velocity gradients modify the dissipation of gas-phase velocity fluctuations, which are no longer characterized by the Kolmogorov length scale, unlike in the case of single-phase turbulence. These mechanisms determine the level

of gas-phase velocity fluctuations $k^{(f)}$ in a particle-laden flow. While these phenomena have been studied for the case of sub-Kolmogorov particles ($d_p < \eta$) (see Balachandar and Eaton (2010), and references therein), they have not been comprehensively studied for large particles ($d_p > \eta$). The level of $k^{(f)}$ consists of both pre-existing turbulent fluctuations in the carrier flow and pseudo-turbulent gas-phase velocity fluctuations due to the presence of particles. Since the mechanisms for the generation and dissipation of these fluctuations are different, it is useful from a modeling viewpoint to distinguish the pseudo-turbulent from the pre-existing turbulent velocity fluctuations in gas-solid suspensions.

Moran and Glicksman (2003) observed experimentally that the presence of particles in circulating fluidized beds produces high levels of velocity fluctuations at dilute solid volume fractions that is significant compared to gas-phase turbulent velocity fluctuations in the absence of particles. The hot wire anemometer technique used by Moran and Glicksman (2003) cannot distinguish the directional components of the velocity fluctuations. Furthermore, it is an intrusive measurement technique, as is the specially designed pitot probe used by Doig and Roper (1967). On the other hand, non-intrusive methods of laser Doppler anemometry (LDA) (Lee and Durst, 1982; Rogers and Eaton, 1991; Sato et al., 1996), and particle image velocimetry (PIV) (Oakley et al., 1997; Kiger and Pan, 2000) are limited to very dilute systems due to the difficulties with optical access in denser gas-solid systems.

An alternative approach to investigate gas-phase velocity fluctuations in gas-solid flows is to use particle-resolved direct numerical simulation (PR-DNS) that provides detailed spatial and temporal information of the flow field. For gas-solid flows with particle diameter greater than the Kolmogorov length scale, PR-DNS is necessary to resolve all the scales of the carrier flow turbulence and the flow scales introduced by the presence of particles. PR-DNS has been used to study the interaction of decaying isotropic turbulence with a single particle (Bagchi and Balachandar, 2004; Burton and Eaton, 2005) or a collection of particles (Zhang and Prosperetti, 2005), particle-laden turbulent channel flow (Uhlmann, 2008), gas-solid flows with upstream turbulence (Xu and Subramaniam, 2010), as well as statistically homogeneous pseudo-turbulent gas-solid flows with a mean slip velocity (Tenneti et al., 2012).

In the current study we perform PR-DNS of homogeneous gas-solid systems with a finite

mean slip velocity in fixed particle assemblies and freely evolving suspensions. The fixed particle assembly simulations are used to determine the relative contribution of turbulent and pseudo-turbulent gas-phase velocity fluctuations to the steady level of $k^{(f)}$. In these simulations the particles are held stationary and a steady flow is established by imposing a mean pressure gradient that corresponds to the desired flow rate. Use of the fixed-bed simulation methodology for gas-solid flows is justified if the configuration of the particles changes very slowly compared to the time it takes to attain mean momentum balance. Xu and Subramaniam (2010) and Tenneti et al. (2012) argued that the timescale over which the particle configuration changes depends on $Re_T = d_p T^{1/2}/\nu^{(f)}$, which is the Reynolds number based on the particle fluctuating velocity characterized by the particle granular temperature T. Since both experiment (Cocco et al., 2010) and PR-DNS (Tenneti et al., 2010) of gas-solid flows show that Re_T is low for high Stokes number suspensions, fixed-particle assemblies have been used as a good approximation to freely evolving suspensions. However, a direct comparison between fixed and freely evolving suspensions at the same solid volume fraction and Reynolds number has not been reported to the best of our knowledge.

In real particle-laden flows, the particles move and collide freely. Numerical simulations of freely evolving suspensions have been performed elsewhere (Yin and Koch, 2007) to study the sedimentation of particles under gravity in the presence of fluid. In these studies the steady mean flow Reynolds number attains a unique value that depends on problem parameters (gas and particle densities, solid volume fraction, gravitational acceleration, etc.). Therefore, in sedimenting suspensions it is not possible to simulate arbitrary Reynolds numbers. However, the simulation of freely evolving suspensions in an accelerating frame of reference (Tenneti et al., 2010) enables us to simulate suspensions at arbitrary Reynolds numbers while maintaining other parameters at fixed values. The results are then compared over a wide range of problem parameters with data from fixed particle assemblies to gain insight into the effect of freely moving particles on gas-phase velocity fluctuations. In addition, we verify the validity of the fixed bed approximation to freely evolving suspensions of high Stokes number particles.

Although PR-DNS is an appropriate tool to investigate particle-laden flows with $d_p > \eta$, they are prohibitively expensive for device-scale calculations. Device-scale calculations require

CFD simulations of multiphase flows (Halvorsen et al., 2003; Sun et al., 2007) that solve averaged equations for mass, momentum and energy with coupling terms corresponding to interphase interactions. The closure of these equations requires modeling of interphase terms and second moments of velocity fluctuations in both phases. In early modeling attempts (Sinclair and Jackson, 1989; Ding and Gidaspow, 1990; Pita and Sundaresan, 1993) gas-phase velocity fluctuations were usually neglected. The main focus was on the interaction of gas and solid phases through their mean velocities, and the effect of fluctuating velocities in the solid phase that contribute to the granular temperature. The neglect of gas-phase velocity fluctuations that were not previously quantified led to considerable uncertainty in the predictive capabilities of models. Experimental evidence of the importance of gas-phase velocity fluctuations resulted in the emergence of a new class of models in which the effect of gas-phase velocity fluctuations was also considered. Among the first to model the effect of gas-phase velocity fluctuations were the one-equation model of Louge et al. (1991) and hte two-equation model of Bolio et al. (1995) for dilute systems of large particles. Later on, more sophisticated models such as the four-equation k-ε model of Simonin (1996) were proposed which are valid for a wide range of volume fraction and Reynolds number. These models are basically extended versions of single-phase k-ε models modified to be used in gas-solid flow, and their validity in this regime of gas-solid flow has not been tested. However, PR-DNS of canonical problems plays a key role in shedding light on the physics governing gas-solid flows. The PR-DNS findings can then be used to propose accurate models. In this regard, Tenneti et al. (2012) quantified the level of gas-phase velocity fluctuations from PR-DNS over a wide range of ϕ and Re_m and proposed an eddy viscosity model.

Recent PR-DNS of gas-solid flows (Uhlmann, 2008; Xu and Subramaniam, 2010; Tenneti et al., 2012) indicate that the gas-phase Reynolds stress is strongly anisotropic. In industrial gas-solid flows, the anisotropy of the velocity fluctuations results in anisotropic heat and scalar transport even in statistically homogeneous suspensions. Therefore, the importance of anisotropy motivates us to quantify the level of anisotropy in gas-solid flows extracted from our PR-DNS data. These anisotropy results in conjunction with the model already proposed for gas-phase velocity fluctuations (Tenneti et al., 2012) can be used to develop a model for the

gas-phase Reynolds stress in gas-solid flows.

The rest of the paper reads as follows. In Section 3.2 the numerical method is described. In Section 3.3 the interaction of initial turbulence and particle assemblies in homogeneous systems is addressed. In Section 3.4 the simulations of freely evolving suspensions are presented. In Section 3.5 the anisotropy of the Reynolds stress is examined, followed by conclusions in Section 3.6.

3.2 Numerical method

Numerical investigation of ga-solid flow with particles larger than the Kolmogorov length scale requires PR-DNS. Several numerical methods have been developed for PR-DNS of gas-solid suspensions (Johnson and Tezduyar, 1997; Peskin, 2002; Prosperetti and Oguz, 2001). In this study, we employ the Particle-Resolved Uncontaminated Fluid Reconcilable Immersed Boundary Method (PUReIBM) introduced by Tenneti et al. (2010), which has been successfully used to extract computational drag laws (Tenneti et al., 2011), and quantify gas-phase velocity fluctuations (Tenneti et al., 2012).

PUReIBM utilizes a regular Cartesian mesh wherein the particle surface is described by a discrete number of points. No-slip and no-penetration boundary conditions (BC) are implemented at these points by adding a forcing term to the momentum equation and generating a fictitious flow inside each particle such that the relative velocity of the fluid comes to rest with respect to the particle motion. The instantaneous mass and momentum equations that are solved in PUReIBM are

$$\nabla \cdot \mathbf{u} = 0, \tag{3.1}$$

and

$$\frac{\partial \mathbf{u}}{\partial t} + \mathbf{S} = -\frac{1}{\rho^{(f)}}\mathbf{g} + \nu^{(f)}\nabla^2\mathbf{u} + \frac{1}{\rho^{(f)}}\mathbf{f} - \mathbf{A}_f, \tag{3.2}$$

respectively, where $\mathbf{u}$ is the instantaneous velocity, $\mathbf{S} = \nabla \cdot (\mathbf{uu})$ is the convective term in conservative form, $\mathbf{g}$ is the pressure gradient, and $\mathbf{f}$ is the immersed boundary (IB) forcing term that accounts for the presence of particles by ensuring the no-slip and no-penetration BCs at the particle-fluid interface. The IB forcing in PUReIBM is non-zero only inside the

solid particle. Thus, the equations in the fluid phase are unmodified and the solution in the fluid phase is not contaminated due to the IB forcing. The simulation of freely evolving suspension in PUReIBM is carried out in an accelerating frame of reference that moves with the mean velocity of particles. In Eq. 3.2 $\mathbf{A}_f$ accounts for the acceleration of the frame of reference (Tenneti et al., 2010).

The computation of IB forcing in PUReIBM is similar to the direct forcing method proposed by Yusof (1996). The IB forcing at the $(n+1)^{\text{th}}$ time-step is specified to cancel the remaining terms in the momentum conservation and force the velocity to its desired value u_i^d at that location:

$$\mathbf{f}^{n+1} = \rho^{(f)} \frac{\mathbf{u}^d - \mathbf{u}^n}{\Delta t} + \rho^{(f)} \mathbf{S}^n + \mathbf{g}^n - \mu^{(f)} \nabla^2 \mathbf{u}^n + \rho^{(f)} \mathbf{A}_f, \tag{3.3}$$

The governing equations in PUReIBM are solved by imposing periodic BCs on fluctuating variables at the boundaries of the computational domain. The velocity field is decomposed into a spatially uniform mean flow that is purely time-dependent and a fluctuating velocity field $\mathbf{u}'$ that is periodic, i.e.,

$$\mathbf{u}(\mathbf{x}, t) = \langle \mathbf{u} \rangle_{\mathcal{V}} (t) + \mathbf{u}'(\mathbf{x}, t), \tag{3.4}$$

where the volumetric mean velocity

$$\langle \mathbf{u} \rangle_{\mathcal{V}} (t) = \frac{1}{\mathcal{V}} \int_{\mathcal{V}} \mathbf{u}(\mathbf{x}, t) dv, \tag{3.5}$$

is obtained by averaging the velocity field over the entire computational domain. Similar decompositions can be written for the non-linear term $\mathbf{S}$, pressure gradient $\mathbf{g}$, and immersed boundary forcing $\mathbf{f}$ terms as well. Substituting the above decompositions in Eqs. 3.1 and 3.2, followed by averaging over the entire computational domain yields the volume-averaged mass and momentum conservation equations. Since the volumetric means are independent of spatial location, mean mass conservation is trivially satisfied. The mean momentum balance in the whole domain is

$$\rho^{(f)} \frac{d \langle \mathbf{u} \rangle_{\mathcal{V}}}{dt} = - \langle \mathbf{g} \rangle_{\mathcal{V}} + \langle \mathbf{f} \rangle_{\mathcal{V}} - \rho^{(f)} \mathbf{A}_f, \tag{3.6}$$

where the volume integrals of convective and diffusive terms are zero because of periodic BCs. The mean IB forcing term $\langle \mathbf{f} \rangle$ is computed by volume-averaging the IB force specified in Eq. 3.3

over the region $\mathcal{V}$. The mean pressure gradient $\langle \mathbf{g} \rangle$ is computed such that we obtain the desired flow rate.

Evolution equations for the fluctuating variables are derived by subtracting Eq. 3.6 from Eq. 3.2. Due to the periodicity of the fluctuating fields, a pseudo-spectral method is used with Crank-Nicolson scheme for the viscous terms and an Adams-Bashforth scheme for the convective terms. A fractional time-stepping method based on Kim and Moin's approach (Kim and Moin, 1985) is used to advance the fluctuating velocities in time. The principal advantage of the PUReIBM approach is that it enables the use of regular Cartesian grids to solve for flow past arbitrarily shaped moving bodies without the need for costly remeshing. In addition, the regularity of the mesh simplifies the parallelization of PUReIBM.

The salient feature of PUReIBM that distinguishes it from other IB methods is that the IB forcing in PUReIBM is non-zero only inside the solid phase and the fluid-phase is uncontaminated by the IB forcing. Therefore the velocity and pressure in the fluid phase is a solution to the unmodified Navier-Stokes equation. In addition, the hydrodynamic force experienced by a particle is computed directly from the stress tensor at the particle surface that is obtained from this uncontaminated fluid flow solution. This feature enables us to directly compare the DNS solution with any random-field theory of multiphase flow (Garg et al., 2011; Tenneti et al., 2011).

Garg et al. (2011) and Tenneti et al. (2011) have shown that PUReIBM is numerically convergent and accurate for DNS of gas-solid flows. The method is validated through a comprehensive set of tests: (i) flow past an isolated sphere (ii) Stokes flow past SC and FCC arrangements (ranging from dilute to close-packed limit) compared with the boundary-integral method of Zick and Homsy (1982), (iii) Stokes flow past random arrays of monodisperse spheres compared with LBM simulations of van der Hoef et al. (2005), (iv) moderate to high Reynolds numbers ($Re_m = 300$) in SC and FCC arrangements compared with LBM simulations of Hill et al. (2001), and (v) high Reynolds number flow past random arrays of monodisperse spheres with ANSYS–FLUENT CFD package.

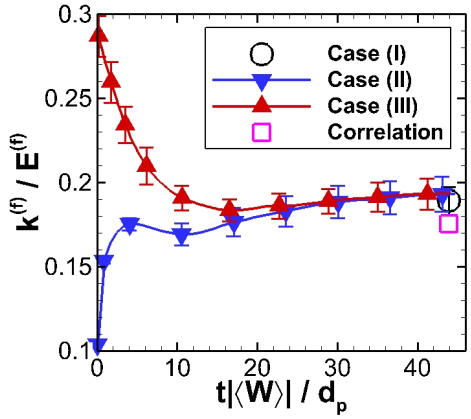

Figure 3.1 Evolution of $k^{(f)}$ normalized with mean flow energy. Symbols ($\bigtriangledown$) correspond to the simulation initialized with an isotropic turbulence. Symbols ($\bigtriangleup$) represent simulation of perturbed velocity field. Symbol ($\bigcirc$) shows the steady value of pseudo-turbulence simulation. Symbol ($\square$) shows the value from the correlation 3.10.

3.3 Gas-phase velocity fluctuations in steady flow past fixed particle assemblies

While the evolution of gas-phase velocity fluctuations due to particles has been studied for zero mean slip (Zhang and Prosperetti, 2005), the mean slip velocity between the phases is non-zero in fluidized beds. PR-DNS of Tenneti et al. (2012) showed the existence of significant gas-phase velocity fluctuations in homogeneous gas-solid systems initialized with a uniform flow under an imposed mean pressure gradient. However, the study did not address the influence of initial turbulence on $k^{(f)}$. Xu and Subramaniam (2010) studied the interaction of a turbulent upstream flow with a fixed particle assembly in an attempt to reproduce the experimental findings of Moran and Glicksman (2003). In their study the upstream flow is initialized with isotropic turbulence and drawn through a uniform configuration of fixed particles by imposing a mean constant pressure gradient. This flow is inhomogeneous in the mean flow direction but gas-phase velocity fluctuations reach a constant value within three particle diameters of entering the bed. The significant result of this study is the enhancement of turbulence as it interacts with solid spheres of the fixed bed.

In the current study, we simulate initially turbulent flow in fixed particle assemblies to quantify the relative magnitude of gas-phase velocity fluctuations arising from turbulent and

pseudo-turbulent sources. A uniform distribution of non-overlapping spheres is generated using the Matérn hard-core point process (Stoyan et al., 1995). This is essentially a Poisson point process for particle centers from which overlapping spheres have been removed using an approach called dependent thinning. In our study, the particle configurations correspond exactly to the uniform distribution in Xu and Subramaniam (2010). To address the level of turbulent and pseudo-turbulent gas-phase velocity fluctuations we consider three types of simulations as follows:

1. Case I initialized with a non-turbulent uniform laminar flow
2. Case II initialized with an isotropic turbulent flow
3. Case III initialized with the steady solution of Case I to which the initial isotropic turbulence of Case II is added

The simulations start by imposing a mean pressure gradient along the mean flow such that the Reynolds number reaches the desired value. The Reynolds number based on the mean slip velocity is defined as

$$Re_m = \frac{|\langle \mathbf{W} \rangle| (1-\phi) d_p}{\nu^{(f)}}, \tag{3.7}$$

with $\langle \mathbf{W} \rangle$ being the mean slip velocity. The mean slip Reynolds number is 50 for all cases. Detailed information of flow parameters is provided in Table 3.1.

The energy in the gas-phase velocity fluctuations $k^{(f)}$ is computed by ensemble-averaging over multiple independent realizations corresponding to different particle configurations:

$$k^{(f)} = \frac{1}{\mathcal{M}} \sum_{\mu=1}^{\mathcal{M}} k_\mu^{(f)}, \tag{3.8}$$

Table 3.1 The numerical and physical parameters of turbulent/pseudo-turbulent simulations.

	ϕ	Re_m	Re_λ	d_p/η	$d_p/\Delta x$	$\mathcal{L}/d_p$
Case I: pseudo-turbulent	0.05	50	–	–	20	12.5
Case II: turbulent	0.05	50	12	5	20	12.5
Case III: Case $I_{s.s.}$+ iso. turb.	0.05	50	–	–	20	12.5

where the number of realizations $\mathcal{M}$ is 4 for all cases. The gas-phase fluctuating velocity energy of each realization $k_\mu^{(f)}$ is

$$k_\mu^{(f)} = \frac{1}{2V^{(f)}} \int_{\mathcal{V}_\mu^{(f)}} u_i''^{(f)} u_i''^{(f)} dV, \tag{3.9}$$

with $u_i''^{(f)}$ being the gas-phase velocity fluctuations defined as $u_i^{(f)} - \left\langle u_i^{(f)} \right\rangle$, $\mathcal{V}_\mu^{(f)}$ being the region occupied by gas-phase in μ^{th} realization, and $V^{(f)}$ is the gas-phase volume.

The first verification we perform is comparing the level of pseudo-turbulent gas-phase velocity fluctuations with a correlation to PR-DNS data for slightly higher volume fractions. Using PR-DNS in the range $0.1 \leq \phi \leq 0.5$ and $0.01 \leq Re_m \leq 300$, Tenneti et al. (2012) showed that the energy in pseudo-turbulent velocity fluctuations is characterized by the following correlation

$$\frac{k^{(f)}}{E^{(f)}} = 2\phi + 2.5\phi(1-\phi)^3 \exp\left(-\phi Re_m^{1/2}\right), \tag{3.10}$$

with $E^{(f)}$ being the mean flow energy defined as $\langle \mathbf{W} \rangle \cdot \langle \mathbf{W} \rangle / 2$. Although there is no simulation data at $\phi = 0.05$ in that work, Fig. 3.1 shows that the value obtained from Eq. 3.10 corresponding to $\phi = 0.05$ for Case I is 0.18, which is in good agreement (less than 10% difference) with the steady value of $k^{(f)}$ from our simulation.

The initial isotropic turbulence in Case II is generated by the method described by Rogallo (1981) for a Taylor microscale turbulent Reynolds number Re_λ of 12 with the energy spectrum function given by Pope (2000). The corresponding Kolmogorov length scale is selected such that the ratio d_p/η is 5. Fig. 3.1 also indicates that for Case II, the level of $k^{(f)}$ starts from the specified initial isotropic turbulence level and increases to the steady state pseudo-turbulent value. The data reveals that the velocity fluctuations arising from the particles in gas-phase are much higher than the turbulent velocity fluctuations for $Re_\lambda = 12$, and the principal contribution to the gas-phase velocity fluctuations is the pseudo-turbulent part.

Since in this study, the configurations and simulation parameters are the same as those chosen by Xu and Subramaniam (2010), we can compare the $k^{(f)}$ between homogeneous simulations of PUReIBM and inflow/outflow simulations of Xu and Subramaniam (2010). In their study, the flow is inhomogeneous along the flow direction and $k^{(f)}$ is reported along the mean flow direction. The level of $k^{(f)}$ increases from the beginning of the bed and represents a 100% increase from the entrance of particle bed and reaches a constant value after an entrance

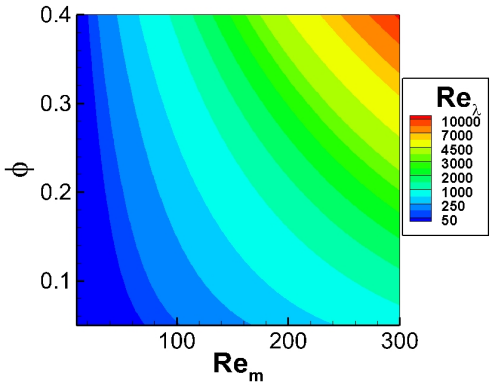

Figure 3.2 The equivalent Taylor microscale turbulent Reynolds number which generates the same pseudo-turbulent level of velocity fluctuations observed in gas-solid flows. The figure corresponds to $d_p/\eta = 5$.

length of $3d_p$. Our homogeneous simulation results are similar for Case II where normalized $k^{(f)}$ starts from an initial value of 0.1 and reaches approximately twice its initial value (0.19) at steady state. This indicates that the enhancement observed by Xu and Subramaniam (2010) is mainly due to the pseudo-turbulent velocity fluctuations, and the steady state value can be characterized by flow parameters ϕ and Re_m as Eq. 3.10.

From these results, it is clear that the turbulent velocity fluctuations will only be important if they are of the same level as, or higher than, the pseudo-turbulent velocity fluctuations. Therefore, it is interesting to determine the Taylor microscale Reynolds number that generates a level of initial turbulence comparable to the steady value of $k^{(f)}$, and to ascertain its scaling with ϕ, d_p/η, and Re_m. The equivalent Re_λ is determined by using the isotropic turbulence scaling relations in single-phase turbulence (Pope, 2000), and employing the relation between Re_L and Re_λ, which is $Re_\lambda = (20Re_L/3)^{1/2}$. In this context, the turbulent Reynolds number Re_L is related to the large eddy and dissipative length scales by the expressions $Re_L = k^{1/2}L/\nu$ and $Re_L^{-3/4} = \eta/L$, respectively. The elimination of large eddy length scale L between these relations, and substitution of single-phase k by the pseudo-turbulent level of $k^{(f)}$ leads to an expression for Re_L as

$$Re_L^{1/2} = \frac{k^{(f)}\eta^2}{\nu^2}. \tag{3.11}$$

The use of Eq. 3.10 for the level of $k^{(f)}$ in above equation and expressing Re_L in terms of Re_λ, a final expression for the equivalent Taylor microscale turbulent Reynolds number is obtained

as

$$Re_\lambda = \sqrt{\frac{20}{3}} \left\{ \phi + 1.25\phi(1-\phi)^3 \exp\left(-\phi Re_m^{1/2}\right) \right\} \left(\frac{\eta}{d_p}\right)^2 \left(\frac{Re_m}{1-\phi}\right)^2. \tag{3.12}$$

This expression shows that the equivalent Re_λ is a function of solid volume fraction, mean slip Reynolds number, and particle diameter to Kolmogorov length scale ratio. The dependence of equivalent Re_λ on ϕ is through the expression for the pseudo-turbulent gas-phase velocity fluctuations $k^{(f)}/E^{(f)}$ in Eq. 3.10. Since this $k^{(f)}$ increases with volume fraction (Tenneti et al., 2012), the equivalent Re_λ also increases. In addition, the quadratic dependence of Re_λ on Re_m indicates that the large eddies associated with the flow structures due to the presence of particles contribute increasingly to the equivalent isotropic Re_λ. The dependency of Re_λ on η/d_p is also represented in Eq. 3.12 by a quadratic term. To observe the influence of d_p/η, we introduce the definition of the Kolmogorov length scale $\eta = (\nu^3/\varepsilon)^{1/4}$ to obtain $d_p/\eta = (\varepsilon d_p^4/\nu^3)^{1/4}$, which shows that increase of d_p/η causes the dissipation of kinetic energy ε to increase dramatically. By maintaining other parameters constant, the large eddy length scale decreases since it is defined as $L = k^{3/2}/\varepsilon$. Thus, the decrease of L results in the attenuation of the turbulent Reynolds number Re_L, which implies a lower equivalent Re_λ. To gain insight into the behavior of equivalent Re_λ, a contour plot of Re_λ for $d_p/\eta = 5$ is presented in Fig. 3.2. This figure reveals that for relatively dense flows at moderate or high mean slip Reynolds numbers, the velocity fluctuations induced by particles are equivalent to high levels of single phase turbulence. Since most PR-DNS of isotropic turbulence are limited to $Re_\lambda \approx 30$ (Burton and Eaton, 2005; Zhang and Prosperetti, 2005), this indicates that even a moderate value of mean slip velocity can easily generate high pseudo-turbulent velocity fluctuations compared to the level of turbulent fluctuations (initial or upstream) in the gas phase.

Case III is basically used to examine the relaxation of turbulence in particle-laden flows. The evolution of $k^{(f)}$ for Case III in Fig. 3.1 shows that the excess amount of $k^{(f)}$ decays and the pseudo-turbulent steady state level of $k^{(f)}$ is recovered. These results showing both attenuation and enhancement of turbulence depending on the initial level of velocity fluctuations indicate that for this choice of ϕ and Re_m, initial turbulent motions in the gas-phase do not influence the steady value of $k^{(f)}$, which corresponds to the pseudo-turbulent fluctuations arising from the interaction of particles with the mean flow. The contour plot in Fig. 3.2 is useful in quantifying

when initial turbulence or the pseudo-turbulent contribution dominates the steady value of $k^{(f)}$. Since the mechanism for generation and dissipation of these contributions to $k^{(f)}$ are different, this provides useful information for the development of predictive multiphase turbulence models in this regime of gas-solid flow. Although the pseudo-turbulent contribution to $k^{(f)}$ studied in this section is comprehensively quantified by Tenneti et al. (2012), the influence of particle movements on $k^{(f)}$ is neglected. Thus, in the following section we study the effect of particle motion on the kinetic energy of the carrier flow.

3.4 Gas-phase velocity fluctuations in freely evolving suspensions

Although fixed beds are good approximations to the particle-laden flows at high particle Stokes number, in reality each sphere moves with an acceleration arising from hydrodynamic and collisional forces. Simulation of freely evolving suspensions enables us to study the effect of physical parameters such as solid to gas density ratio and coefficient of restitution, in addition to solid volume fraction and Reynolds number that are used to characterize fixed bed simulations. In freely evolving suspensions, particles move under the influence of hydrodynamic and collisional forces. In PUReIBM the particles are represented in a Lagrangian frame of reference at time t by $\{\mathbf{X}^{(i)}(t),\ \mathbf{V}^{(i)}(t)\ i = 1...N_p\}$ with $\mathbf{X}^{(i)}(t)$ and $\mathbf{V}^{(i)}(t)$ being the position and velocity of i^{th} particle respectively, and N_p being the total number of particles. The position and translational velocity of i^{th} particle evolve according to Newton's second law as

$$\frac{d\mathbf{X}^{(i)}(t)}{dt} = \mathbf{V}^{(i)}(t), \tag{3.13}$$

$$m\frac{\mathbf{V}^{(i)}(t)}{dt} = \mathbf{B} + \mathbf{F}_h^{(i)}(t) + \sum_{\substack{j=1 \\ j\neq i}}^{N_p} \mathbf{F}_{ij}^{(c)}(t) \tag{3.14}$$

where $\mathbf{B}$ is any external body force, $\mathbf{F}_h^{(i)}$ is the hydrodynamic force (calculated from the velocity and pressure fields at the particle surface) and $\mathbf{F}_{ij}^{(c)}$ is the contact force on the i^{th} particle as a result of collision with j^{th} particle. Particle-particle interactions are treated using soft-sphere collisions based on a linear spring-dashpot contact mechanics model that was originally proposed by Cundall and Strack (1979) (details are given in Appendix A). The hydrodynamic and

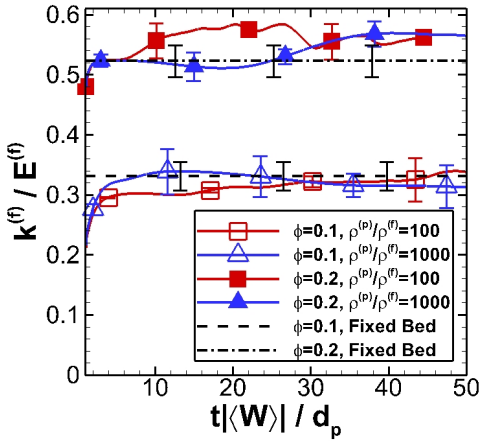

Figure 3.3 Evolution of $k^{(f)}$ normalized with mean flow energy for elastic particles with different ϕ and $\rho^{(p)}/\rho^{(f)}$.

contact forces computed at each time step are then used to evolve the position and translational velocity of particles by means of Eqs. 3.13 and 3.14, respectively.

The formulation of PUReIBM in an accelerating frame of reference enables the simulation of not just sedimenting suspensions, but arbitrary mean slip values while maintaining average particle motion at rest in the accelerating frame. In other words, the use of accelerating frame of reference facilitates examining the influence of each flow parameter while maintaining other parameters constant.

In our freely evolving suspension study, all the simulations are performed at $Re_m = 20$ with two independent realizations for each case. The influence of solid volume fraction is studied by simulating two volume fractions $\phi = 0.1$ and 0.2. The simulations are initialized with a uniform mean flow for the gas phase and zero granular temperature for the solid phase, and carried out until a steady state solution is obtained in terms of $k^{(f)}$. To investigate the effect of particle to gas density ratio we simulated density ratios $\rho^{(p)}/\rho^{(f)} = 100$ and 1000. The comparison of $k^{(f)}$ for the two density ratios with elastic particles indicates that the level of gas-phase velocity fluctuations is not influenced by particle densities significantly as shown in Fig. 3.3. In this figure $k^{(f)}$ increases rapidly and then attains a relatively constant value. The evolution of $k^{(f)}$ is also compared with fixed bed results at the same Reynolds number and solid volume fractions represented by dashed lines in the figure. The difference of $k^{(f)}$ in freely evolving suspensions from its value in the corresponding fixed bed is less than 10%.

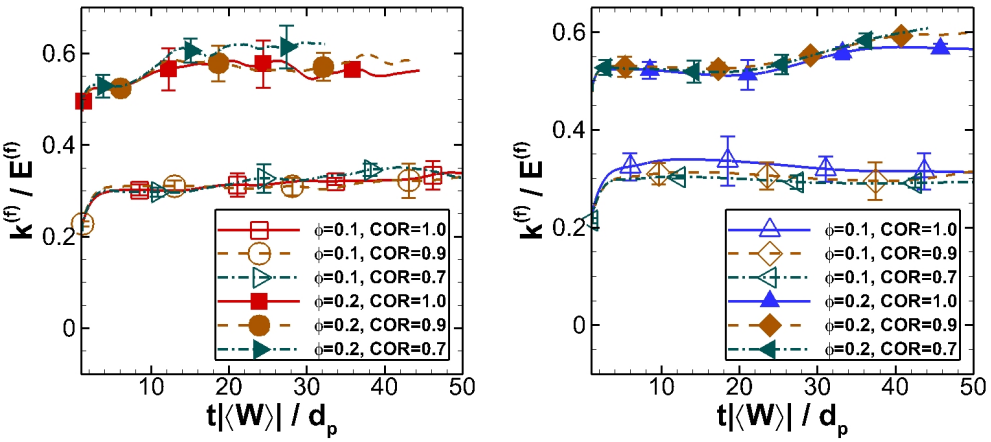

(a) $\rho^{(p)}/\rho^{(f)} = 100$ (b) $\rho^{(p)}/\rho^{(f)} = 1000$

Figure 3.4 Comparison of $k^{(f)}$ normalized with mean flow energy among elastic and inelastic cases.

This establishes the validity of using fixed bed simulations as an approximation to high Stokes number suspensions undergoing elastic collisions, which was employed in earlier studies (Xu and Subramaniam, 2010; Tenneti et al., 2012).

In freely evolving suspensions with inelastic particle collisions, the energy of the system is dissipated by collisional dissipation among particles as well as the viscous dissipation of the carrier flow. To investigate the effect of the coefficient of restitution (COR) on $k^{(f)}$, we selected three values 1.0, 0.9, and 0.7 for this parameter. The comparison of $k^{(f)}$ for particles with different CORs, presented in Fig. 3.4, indicates that $k^{(f)}$ is not very sensitive to COR and the differences are not statistically significant, especially for the lower volume fraction. In addition, as Figs. 3.4(a) and 3.4(b) show, the density ratio has negligible effect on the level of $k^{(f)}$ for inelastic particles. Similar to the results of elastic particles, the level of $k^{(f)}$ is in good agreement with those of fixed beds with a maximum difference of 10% for the higher volume fraction. The weak dependence of $k^{(f)}$ on inelasticity of particles further shows the validity of using fixed beds as an approximation to high Stokes number suspensions.

The independence of $k^{(f)}$ on COR indicates that these suspensions belong to a regime that is dominated by viscous dissipation as opposed to collisionally dissipative regime (Sangani et al., 1996). To precisely characterize the regime of the gas-solid flows examined in this study, we quantify the ratio of time taken by gas-phase forces to affect particle motions t_{fluid} to the

average time between collisions t_{coll} (Wylie et al., 2003). The fluid timescale is defined as

$$t_{\text{fluid}} = \frac{\sqrt{3T}}{\sigma_A}, \tag{3.15}$$

where σ_A characterizes the standard deviation in particle accelerations. The mean collisional timescale is computed from the inverse of Enskog collisional frequency (Chapman and Cowling, 1953), that is

$$t_{\text{coll}} = \frac{2}{G\sqrt{T}}, \tag{3.16}$$

with G defined as $8d_p^2 n\sqrt{\pi/m}g(d_p)$ in which n is the particle number density, and $g(d_p)$ is the radial distribution function of particle assembly at contact. From Eqs. 3.15 and 3.16, the fluid to collisional timescale ratio is

$$\frac{t_{\text{fluid}}}{t_{\text{coll}}} = \frac{\sqrt{3}GT}{2\sigma_A}, \tag{3.17}$$

which is quantified for the cases simulated in this study, and ranges from 0.19 to 0.9. This confirms that the time required for the gas-phase stresses to significantly influence the particles motion is less than the mean time between the collisions ($t_{\text{fluid}} < t_{\text{coll}}$). In other words, these gas-particle systems are dominated by viscous forces, and the energy loss due to collisional dissipations does not affect significantly the evolution of $k^{(f)}$. Thus, the energy of gas-phase fluctuating velocities evolves in a manner similar to fixed bed assemblies.

To better understand the transfer of energy between two phases for freely moving particles, it is useful to investigate the evolution equations of fluctuating energies in both gas and solid phases. This also helps understand the effect of COR through the collisional dissipation. The evolution of $k^{(f)}$ for a homogeneous suspension is given by (Xu and Subramaniam, 2006; Pai and Subramaniam, 2009; Tenneti et al., 2012)

$$\underbrace{\rho^{(f)}(1-\phi)\frac{d}{dt}k^{(f)}}_{\text{unsteady term}} = \underbrace{\left\langle u_i''^{(f)}\tau_{ji}n_j^{(f)}\delta\left(\mathbf{x}-\mathbf{x}^{(\mathbf{I})}\right)\right\rangle}_{\Pi^{(f)}} - \underbrace{2\mu^{(f)}\left\langle I^{(f)}S_{ij}S_{ij}\right\rangle}_{\varepsilon^{(f)}}, \tag{3.18}$$

where $\rho^{(f)}$ is the gas-phase density, $\boldsymbol{\tau}$ is the stress tensor, $\mathbf{n}^{(f)}$ is the unit normal vector pointing outward from the gas phase into the solid phase, $\delta\left(\mathbf{x}-\mathbf{x}^{(\mathbf{I})}\right)$ is the Dirac delta function representing the gas-solid interface, $\mu^{(f)}$ is the gas-phase dynamic viscosity, and $\mathbf{S}$ is the strain rate tensor. The interphase turbulent kinetic energy (TKE) transfer $\Pi^{(f)}$ in Eq. 3.18 arises

from the fluctuating velocity-stress tensor correlation which is non-zero at gas-solid interface due to the Dirac delta function. The viscous dissipation in the gas phase $\varepsilon^{(f)}$ is a sink of energy since $S_{ij}S_{ij}$ is always a positive quantity (Tenneti et al., 2012). On the other hand, the evolution equation of solid-phase fluctuating kinetic energy $k^{(p)}$ for a homogeneous system is

$$\underbrace{\rho^{(p)}\phi\frac{d}{dt}k^{(p)}}_{\text{unsteady term}} = \underbrace{\left\langle u_i''^{(p)}\tau_{ji}n_j^{(p)}\delta\left(\mathbf{x}-\mathbf{x}^{(\mathbf{I})}\right)\right\rangle}_{\Pi^{(p)}} - \underbrace{\Gamma_{\text{coll}}}_{\text{collisional dissipation}} . \tag{3.19}$$

In this equation, $k^{(p)}$ is defined as $\left\langle \mathbf{u}''^{(p)}\cdot\mathbf{u}''^{(p)}\right\rangle/2$ where $\mathbf{u}''^{(p)}$ is the solid-phase velocity being $\mathbf{u}^{(p)}-\langle\mathbf{u}\rangle$. In addition, $\rho^{(p)}$ is the solid-phase density, and $\mathbf{n}^{(p)}$ is the unit normal vector pointing outward from the particle into the gas phase. Note that the unit normal vectors are related to each other as $\mathbf{n}^{(p)}=-\mathbf{n}^{(f)}$. It has been shown that the correlation of the fluctuating particle acceleration with the fluctuating particle velocity $\Pi^{(p)}$ acts as both source and sink of particle kinetic energy (Koch, 1990; Koch and Sangani, 1999; Tenneti et al., 2010).

The kinetic energy of the two-phase mixture e_m is defined as $\rho^{(f)}(1-\phi)k^{(f)}+\rho^{(p)}\phi k^{(p)}$. The mixture kinetic energy evolution equation is obtained by adding Eqs. 3.18 and 3.19 as

$$\frac{de_m}{dt} = \Pi^{(f)}+\Pi^{(p)}-\varepsilon^{(f)}-\Gamma_{\text{coll}}. \tag{3.20}$$

The principle of conservative interphase TKE transfer introduced by Xu and Subramaniam (2007) implies that the summation of interphase TKE transfer between the two phases ($\Pi^{(f)}+\Pi^{(p)}$) reduces to the inner product of the mean slip $\langle\mathbf{W}\rangle$ and the mean momentum transfer $\langle\mathbf{F}\rangle$, such that

$$\frac{de_m}{dt} = \underbrace{\langle W_i\rangle\langle F_i\rangle}_{\Pi_m} - \varepsilon^{(f)}-\Gamma_{\text{coll}}. \tag{3.21}$$

For random assemblies, since the mean slip velocity is aligned with the mean interphase momentum transfer (Hill et al., 2001; Tenneti et al., 2010), the resultant interphase TKE transfer Π_m is positive and represents a source of energy, while the viscous dissipation and the collisional dissipation are sinks of energy. At steady state the terms on the right-hand-side of Eq. 3.21 should balance each other. The Π_m term is computed directly from the DNS data by inner product of the mean slip and the mean drag force measured from the integration of the stress tensor at particle surface. The viscous dissipation is also computed directly from the DNS by

the expression given by Tenneti et al. (2012), that is

$$\varepsilon^{(f)} = \frac{1}{V^{(f)}} \int_{\mathcal{V}} I^{(f)} 2\mu S_{ij} S_{ij} dV. \tag{3.22}$$

The collisional dissipation of the system is estimated from the expression given by Sangani et al. (1996) as

$$\Gamma_{\text{coll}} = \frac{24}{d_p \pi^1/2} (1-e)\, \rho^{(p)} \phi g(d_p) T^{3/2} \tag{3.23}$$

where e is the COR.

The budget analysis of Eq. 3.21 in Fig. 3.5 indicates that for these suspensions that start from rest and attain a relatively low steady state granular temperature, the principal balance of terms is between Π_m and $\varepsilon^{(f)}$, while Γ_{coll} is negligible. The balance of energy implies that the level of collisional dissipation in gas-solid suspensions with low granular temperature ($Re_T/Re_m \approx 0.12$) is not significant compared to interphase TKE transfer and viscous dissipation. We also simulated cases with higher initial granular temperature (twice the steady Reynolds number based on granular temperature; results not shown here) and found that although Γ_{coll} is initially higher than at the steady state, it does not affect the steady $k^{(f)}$ and $k^{(p)}$. Thus, the inelasticity of particles does not influence the overall level of energy in the system and the level of $k^{(f)}$ will be similar for flows with different COR. This finding suggests that the model proposed for fixed beds is applicable to freely evolving suspensions of gas-solid flow as well. In the following section, we quantify the anisotropy of the gas-phase Reynolds stress in fixed beds.

3.5 Reynolds stress tensor of pseudo-turbulent gas-phase velocity fluctuations

The gas-phase Reynolds stress is defined as

$$R_{ij}^{(f)} = \left\langle u_i''^{(f)} u_j''^{(f)} \right\rangle, \tag{3.24}$$

and its trace represents the level of gas-phase velocity fluctuations $k^{(f)}$. The presence of particles introducing anisotropy in the gas-phase Reynolds stress modifies the structure of the

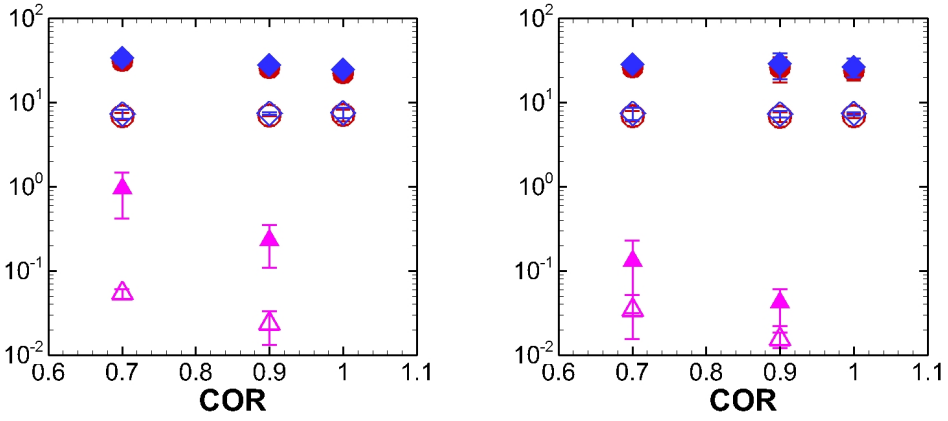

(a) $\rho^{(p)}/\rho^{(f)} = 100$ (b) $\rho^{(p)}/\rho^{(f)} = 1000$

Figure 3.5 The balance of mixture energy equation terms (Eq. 3.21) normalized with $\mu^{(f)}(\mid \langle \mathbf{W} \rangle \mid /d_p)^2$. Π_m (◯), $\varepsilon^{(f)}$ (◇), Γ_{coll} (△); hollow symbols ($\phi = 0.1$), filled symbols ($\phi = 0.2$).

carrier phase (Uhlmann, 2008; Xu and Subramaniam, 2010; Tenneti et al., 2012). The gas-phase anisotropy tensor

$$b_{ij}^{(f)} = \frac{R_{ij}^{(f)}}{2k^{(f)}} - \frac{1}{3}\delta_{ij}, \tag{3.25}$$

is quantified for the fixed-bed particle configurations considered in this study. It is observed in aforementioned studies that flow structures extend in the streamwise direction. Therefore, it is logical to compute the Reynolds stress and the corresponding anisotropy along the streamwise (parallel to mean slip) and spanwise (perpendicular to mean slip) directions which are presented in Figs. 3.6(a) and 3.6(b), respectively. The results indicate that the cross-correlation of velocity fluctuations are negligible (not shown here) and the normal component in the parallel direction is dominant compared to the other normal components in the perpendicular direction. Hence, the state of pseudo-turbulent gas-phase velocity fluctuations is axisymmetric (Pope, 2000).

An accurate model for the Reynolds stress should capture the behavior of anisotropy with flow parameters. Fig. 3.6 indicates that the level of anisotropy increases with Re_m from Stokes flow to moderate Reynolds numbers (ranging from 10 to 40) and then smoothly decreases. We hypothesize that this variation in anisotropy is related to the ratio of the length scale associated with gas-phase velocity fluctuations to the local average interparticle spacing. These length scales are quantified using our simulations.

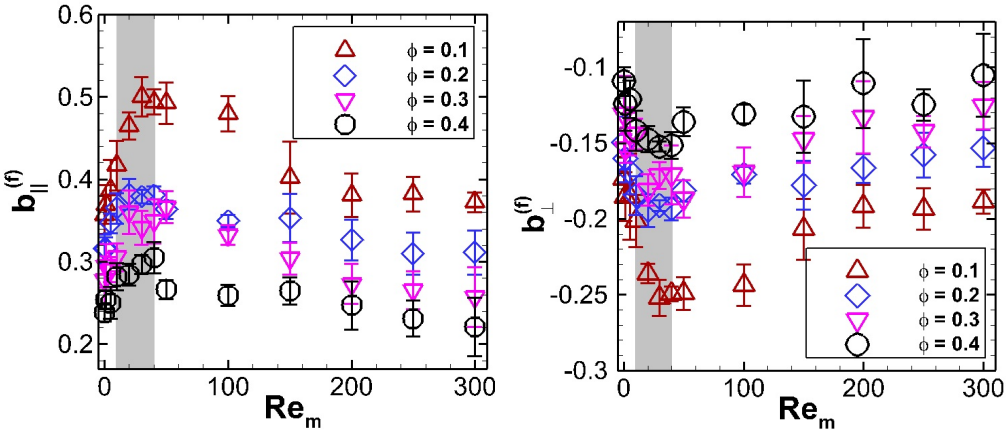

(a) (b)

Figure 3.6 Deviatoric tensor components are shown for different ϕ and Re_m obtained from fixed bed simulations. The shaded region shows where the maximum of anisotropy occurs.

Increase of Reynolds number from low Re_m flow initiates the separation of boundary layer around particles and a standing eddy forms behind spheres with a characteristic length (Pruppacher et al., 1970) which is a source of anisotropy in gas-phase Reynolds stress (Yusof, 1996; Uhlmann, 2008). However, defining an appropriate length scale for gas-phase velocity fluctuations in a random particle assembly is not straightforward since the wakes are affected by the presence of neighbor particles. We use the Eulerian two-point correlation of gas-phase velocity fluctuations to define a characteristic length for gas-phase velocity fluctuations $L_{\parallel}$ as follows:

$$L_{\parallel} = \frac{1}{R_{\parallel}(0)} \int_0^{\infty} R_{\parallel}(r) dr, \tag{3.26}$$

where $R_{\parallel}(r)$ is

$$R_{\parallel}(r) = \frac{1}{V^{(f)}} \int_{\mathcal{V}^{(f)}} \mathbf{u}_{\parallel}^{\prime\prime(f)}(\mathbf{x}) \cdot \mathbf{u}_{\parallel}^{\prime\prime(f)}(\mathbf{x} - \mathbf{r}) dV, \tag{3.27}$$

the two-point correlation in the parallel direction. This gas-phase velocity fluctuations length scale shown in Fig. 3.7 decreases with Re_m due to the fact that the flow structures become finer and less correlated to other surrounding structures. In addition, increase of solid volume fraction makes the gas-phase velocity fluctuations less spatially correlated due to the influence of near particles, and hence the length scale decreases.

We use the radial distribution function $g(r)$ to define a characteristic local interparticle

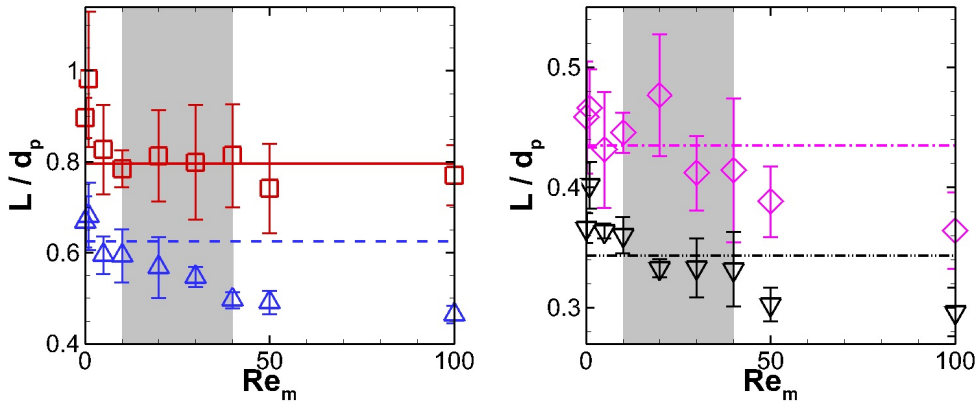

(a) $\phi = 0.1$ (□), $\phi = 0.2$ (△) (b) $\phi = 0.3$ (◇), $\phi = 0.4$ (▽)

Figure 3.7 Symbols show length scale of gas-phase velocity fluctuations, while the straight lines show the corresponding local interparticle spacing. The shaded region shows where the maximum of anisotropy occurs.

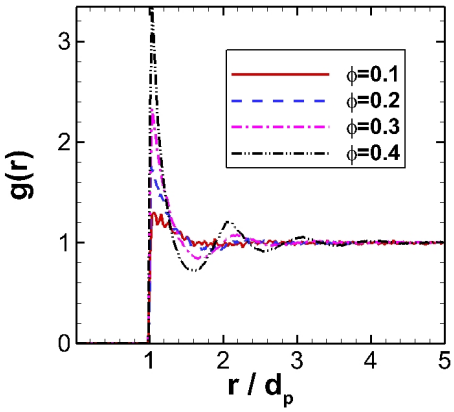

Figure 3.8 Radial distribution function estimated from 100 realizations for different ϕ.

spacing within a neighborhood of a test particle. Note that other studies used a similar approach to compute the nearest neighbor distance for point particles (Hertz, 1909) and finite size particles (Torquato et al., 1990) in random particle arrangements. The radial distribution function is shown in Fig. 3.8 for different volume fractions. The radial distribution is the probability of finding a particle at separation r given that there is a particle at the coordinate origin. By assuming a spherical shell of volume $4\pi r^2 \delta r$ at separation r, the number of particles in the shell is $2\pi N_p n g(r) r^2 \delta r$. Thus, we compute the local interparticle spacing of the suspension

using the expression

$$\frac{L_{int}}{d_p} = \frac{1}{d_p} \frac{\int_{d_p}^{R} g(r) r^2 l f(l) dr}{\int_{d_p}^{R} g(r) r^2 f(l) dr}, \tag{3.28}$$

which is a weighted average of distances among particles in a spherical shell between the minimum separation d_p and R. In Eq. 3.28, l is the surface to surface distance defined as $r - d_p$, and $f(l)$ is a weight function. We choose R as the second peak of $g(r)$, which includes all particles in the local neighborhood of the test particle. The weight function is assumed to have the form $1/l^p$ with $p \geq 0$. Note that the choice of $p = 0$ causes L_{int} to be equally weighted by neighbor particles, while choosing higher values for p preferentially weights the most proximate particles. We select $p = 1$, a value that takes into account the importance of all particles in the region between d_p and R in a manner where proximate particles contribute more to the local interparticle spacing.

The results indicate that the local interparticle spacing (shown as straight lines in Fig. 3.7) intersect the length scales of gas-phase velocity fluctuations at the Reynolds numbers where the anisotropy starts to decrease (Fig. 3.6). At low Reynolds numbers, flow structures formed behind particles elongate with Re_m that give rise to the increase of anisotropy. After moderate Reynolds numbers ($10 \leq Re_m \leq 40$) the wakes become as large as the gaps among particles and are broken up due to interaction with neighbor spheres. Thus, the anisotropy is characterized by the ratio of gas-phase velocity fluctuations length scale to local interparticle spacing. The break up of elongated structures redistributes the fluctuating velocities energy among Reynolds stress components and decreases the anisotropy.

It is also observed that the increase of solid volume fraction causes an attenuation in the level of anisotropy. Increase of solid volume fraction lessens the local interparticle gaps and does not allow the formation of distinct wake wake structures, leading to the decrease of anisotropy. This is confirmed in Fig. 3.7 since the length scale of gas-phase velocity fluctuations decreases with volume fraction. Breault et al. (2008) also reported that the axial solid dispersion coefficient of particles in a particle-laden flow decreases with volume fraction, which is interpreted as indication that $R_{||}$ decreases, while $R_{\perp}$ increases, and our data is in agreement with this trend observed in experiments.

3.6 Conclusion

In this work we characterized the fluctuations in gas-phase velocity using PR-DNS of steady flow at finite Reynolds number (based on the mean slip velocity) in fixed particle beds and freely evolving gas-solid suspensions. The evolution of initially isotropic turbulence in a fixed particle bed with mean slip reveals that for the solid volume fraction and Reynolds number considered in this study, the gas-phase velocity fluctuations arising from the presence of particles always relax to their pseudo-turbulent level quantified by Tenneti et al. (2012), irrespective of the level of initial turbulence. The initial level of turbulence required to match the level of pseudo-turbulent velocity fluctuations is estimated to be very high, e.g. at $Re_m = 100$, $\phi = 0.2$ and $d_p/\eta = 5$, the equivalent Re_λ is 320. Therefore, the principal mechanism for producing gas-phase velocity fluctuations in particle-laden flows with $d_p/\eta > 1$ e.g. fluidized beds, is the interaction of gas and solid phases through the mean slip velocity. Simulations of freely evolving suspensions indicate that $k^{(f)}$ is a strong function of volume fraction, similar to observations in fixed beds. The change of particle density for high Stokes number particles does not significantly change the level of $k^{(f)}$ since the time required for the particle configuration to change is longer than the momentum relaxation time. In addition, the variation of inelasticity does not substantially affect $k^{(f)}$ since viscous dissipation in these systems dominates collisional dissipation. The current study confirms previous findings (Uhlmann, 2008; Xu and Subramaniam, 2010; Tenneti et al., 2012) that the Reynolds stress is highly anisotropic and axisymmetric along the mean slip. Over a wide range of volume fraction ($0.1 \leq \phi \leq 0.4$) the anisotropy increases with Reynolds number as the flow structures form and elongate in the mean slip direction. As Re_m increases in the range $10 \leq Re_m \leq 40$, these structures are affected by neighbor particles that causes them to decorrelate over length scales smaller than local interparticle spacing, resulting in attenuation of anisotropy. Increase of the volume fraction also decreases the local interparticle gaps and flow structures are broken up leading to attenuation of anisotropy. This work gains insight into the nature of gas-phase velocity fluctuations in gas-solid flows that can be used to propose a model for the Reynolds stress due to the pseudo-turbulent gas-phase velocity fluctuations in homogeneous suspensions.

CHAPTER 4. CONCLUSIONS AND FUTURE WORK

4.1 Conclusion

In this study, particle-resolved direct numerical simulation (PR-DNS) was used to address the behavior of gas-phase velocity fluctuations in gas-solid flows, in particular the fluidized beds. The specific findings of the study are as follows:

1. The contribution of turbulent and pseudo-turbulent velocity fluctuations to the steady level of $k^{(f)}$ was determined by simulating a homogeneous gas-solid suspension initialized with both uniform and turbulent flows. The results show that the velocity fluctuations in such systems are due to the interaction of large particles with the mean slip velocity, and that the pre-existing turbulence in the carrier flow is insignificant.

2. A high level of pre-existing turbulence is required to generate the same level of pseudo-turbulent gas-phase velocity fluctuations in gas-solid flows.

3. PR-DNS of freely evolving suspensions with elastic particles indicate that the level of $k^{(f)}$ is in good agreement with the fixed bed values at the same solid volume fraction and Reynolds number for high Stokes number particles. The main reason is that the time required for particle configuration to change is longer than the momentum relaxation time.

4. The variation of inelasticity of particles in freely evolving suspensions does not influence the level of $k^{(f)}$. The balance of energy is generally between viscous dissipation and interphase TKE transfer term, and the low level of collisional dissipation is negligible. Therefore, flow is dominated by viscous forces rather than the collisional forces.

5. The gas-phase Reynolds stress tensor is decomposed into isotropic and anisotropic parts. The Reynolds stress is highly anisotropic along the mean slip velocity and becomes axi-symmetric.

6. Anisotropy of gas-phase velocity fluctuations increases with the Reynolds number to the range $10 \leq Re_m \leq 40$, and then decreases. This observation is characterized by local interparticle spacing and the length scale of gas-phase velocity fluctuations.

7. Anisotropy decreases with increasing ϕ since the wake structures responsible for anisotropy in the gas-phase are broken up by the presence of particles at higher solid volume fractions.

4.2 Future work

In this study, the importance of particle-induced gas-phase pseudo-turbulent velocity fluctuations at steady state is addressed. By investigating the evolution of energy balance among the terms in the transport equation of $k^{(f)}$ in canonical gas-solid flows, a better understanding of mechanisms governing the flow characteristics is obtained. The data collected from this study can be incorporated into any multiphase turbulent flow model, such as equilibration of energy model (Xu and Subramaniam, 2006), consisting of evolution equations for fluctuating velocities and dissipation rates in both phases. In this study we considered uniform configuration of particle assemblies. It is of interest to study the effect of particle clusters on the gas-phase velocity fluctuations and characterize the flow behavior of these mesoscale structures. In addition, current homogeneous suspensions can be extended to homogeneous shear flows where the mean velocity gradients are non-zero. The existence of the mean velocity gradient introduces a new mechanism for generating gas-phase velocity fluctuations. The results shed additional light on the physics of gas-solid flow in fluidized beds, and can be used for model development.

APPENDIX A. PARTICLE MOTION EQUATIONS IN PUReIBM

In the soft-sphere approach, the contact mechanics between two overlapping particles is modeled by a system of springs and dashpots in both normal and tangential directions. The spring causes colliding particles to rebound, and the dashpot mimics the dissipation of kinetic energy due to inelastic collisions. The spring stiffness coefficients in the tangential and normal directions are k_t and k_n, respectively. Similarly, the dashpot damping coefficients in the tangential and normal directions are η_t and η_n, respectively. The spring stiffness and dashpot damping coefficients are related to the coefficient of restitution and the coefficient of friction (Garg et al., 2010).

The particles considered in this study are assumed to be frictionless. Thus the tangential component of the contact force is zero. Therefore, only normal component of the contact force $\mathbf{F}_{\mathbf{n}ij}$ is considered at time t which is given by

$$\mathbf{F}_{n_{ij}} = k_n \delta_{ij} \mathbf{n}_{ij} - \frac{m}{2} \eta_n \mathbf{V}_{n_{ij}}, \tag{A.1}$$

where δ_{ij} is the overlap between the particles computed using the relation

$$\delta_{ij} = d_p - \mid \mathbf{X}^{(i)} - \mathbf{X}^{(j)} \mid, \tag{A.2}$$

and $\mathbf{V}_{n_{ij}}$ is the relative velocity in the normal direction that is defined using

$$\mathbf{V}_{n_{ij}} = \left[\left(\mathbf{V}^{(i)} - \mathbf{V}^{(j)} \right) \cdot \hat{\mathbf{r}}_{ij} \right] \hat{\mathbf{r}}_{ij}. \tag{A.3}$$

The normal vector $\hat{\mathbf{r}}_{ij}$ is the unit vector along the line of contact pointing from particle i to particle j.

APPENDIX B. CONVERGENCE OF VISCOUS DISSIPATION IN PUReIBM

The accuracy of a numerical method depends strongly on the independence of results relative to the computational grid. As mentioned in Chapter 2, convergence of PUReIBM is analyzed using drag force (Tenneti et al., 2011) and gas-phase velocity fluctuations (Tenneti et al., 2012). Since the evolution of fluid-phase velocity fluctuations is significantly affected by viscous dissipation, we focus on the convergence test of $\varepsilon^{(f)}$ in this section. A detailed derivation of $k^{(f)}$ evolution equation for a homogeneous system is presented elsewhere (Xu and Subramaniam, 2006, 2007; Pai and Subramaniam, 2009; Tenneti et al., 2012). However, for the sake of completeness, this equation is explained in the following section. Then, the numerical convergence test results for the dissipation are presented.

B.1 Evolution equation of gas-phase velocity fluctuations in a homogeneous gas-solid suspension

The kinetic energy of fluctuating velocities is obtained by half the trace of the Reynolds stress tensor. In an Eulerian-Eulerian approach, the evolution equation of kinetic energy in phase α is (Pai and Subramaniam, 2009)

$$\phi^{(\alpha)}\rho^{(\alpha)}\frac{\partial k^{(\alpha)}}{\partial t} + \phi^{(\alpha)}\rho^{(\alpha)}\left\langle u_j^{(\alpha)}\right\rangle \frac{\partial k^{(\alpha)}}{\partial x_j} + \phi^{(\alpha)}\rho^{(\alpha)}\frac{\partial}{\partial x_j}\left\langle u_i''^{(\alpha)}u_i''^{(\alpha)}u_j''^{(\alpha)}\right\rangle =$$
$$-\phi^{(\alpha)}\rho^{(\alpha)}\left[\left\langle u_i''^{(\alpha)}u_j''^{(\alpha)}\right\rangle \frac{\partial\left\langle u_i^{(\alpha)}\right\rangle}{\partial x_j}\right] + \left\langle u_i''^{(\alpha)}\frac{\partial}{\partial x_j}\left(I^{(\alpha)}\tau_{ji}\right)\right\rangle + \left\langle u_i''^{(\alpha)}M_i^{(\alpha)}\right\rangle, \quad \text{(B.1)}$$

where $\langle . \rangle$ denotes the ensemble average, $I^{(\alpha)}$ is an indicator function being *one* if the position lies on phase α, and *zero* otherwise, and $M_i^{(\alpha)}$ is the interphase momentum transfer. For a statically homogeneous gas-solid flow, the spatial derivative of mean quantities is zero. Thus,

the evolution equation for the kinetic energy of gas-phase velocity fluctuations reduces to

$$\underbrace{(1-\phi)\rho^{(f)}\frac{\partial k^{(f)}}{\partial t}}_{\text{unsteady term}} = \underbrace{\left\langle u_i''^{(f)} M_i^{(f)} \right\rangle}_{\Pi^{(f)}} + \underbrace{\left\langle u_i''^{(f)} \frac{\partial}{\partial x_j}\left(I^{(f)}\tau_{ji}\right)\right\rangle}_{\varepsilon^{(f)}}. \tag{B.2}$$

The first term on the right-hand-side is the gas-phase interphase TKE transfer $\Pi^{(f)}$, while the second term is usually modeled as the dissipation of gas-phase velocity fluctuations $\varepsilon^{(f)}$.

Interphase TKE transfer is the fluid-phase velocity fluctuations-interphase momentum transfer covariance. For flows with no interphase mass transfer, the interphase momentum transfer in the gas-phase is

$$M_i^{(f)} = -\tau_{ji}\frac{\partial I^{(f)}}{\partial x_j}. \tag{B.3}$$

The interphase momentum transfer can be simplified by using the expression for the gradient of the indicator function (Drew and Passman, 1998)

$$\frac{\partial I^{(f)}}{\partial x_j} = -n_j^{(f)}\delta(\mathbf{x}-\mathbf{x}^{(I)}), \tag{B.4}$$

where $\mathbf{n}^{(f)}$ is the unit normal at the phase interface pointing outward. The Dirac delta function δ indicates the momentum transfer term is only non-zero at the gas-solid interface. Substituting Eq. B.4 into Eq. B.3 results in the final expression for the interphase momentum transfer term as

$$M_i^{(f)} = \tau_{ji}n_j^{(f)}\delta(\mathbf{x}-\mathbf{x}^{(I)}). \tag{B.5}$$

Conversely, the instantaneous gas-phase and solid-phase velocities are the same at gas-particle interface, i.e. $\mathbf{u}^{(f)} = \mathbf{u}^{(p)}$. By decomposing these velocities into the mean and fluctuating parts, an expression for the gas-phase velocity fluctuation at the interface is obtained as

$$u_i''^{(f)} = u_i''^{(p)} + \left\langle u_i^{(p)} \right\rangle - \left\langle u_i^{(f)} \right\rangle. \tag{B.6}$$

We focus on fixed particle assemblies where the particle configuration does not change in response to hydrodynamic forces, implying that the particle velocity fluctuation $\left\langle \mathbf{u}''^{(p)} \right\rangle$ is zero. Additionally, by employing the definition of the mean slip velocity $\langle \mathbf{W} \rangle = \left\langle \mathbf{u}^{(f)} \right\rangle - \left\langle \mathbf{u}^{(p)} \right\rangle$, the fluid-phase velocity fluctuation at gas-particle interface reduces to

$$u_i''^{(f)} = -\langle W_i \rangle. \tag{B.7}$$

Using Eqs. B.5 and B.7 for the definition of $\Pi^{(f)}$ and noting that $\mathbf{n}^{(f)} = -\mathbf{n}^{(p)}$, the interphase TKE transfer is obtained as

$$\left\langle u_i''^{(f)} \tau_{ji} n_j^{(f)} \delta(\mathbf{x} - \mathbf{x}^{(I)}) \right\rangle = \langle W_i \rangle \left\langle \tau_{ji} n_j^{(p)} \delta(\mathbf{x} - \mathbf{x}^{(I)}) \right\rangle, \tag{B.8}$$

the inner product of the mean slip velocity and the total drag force acting at the particle surface. The interphase TKE transfer is positive since the mean slip velocity is aligned with the mean interphase momentum transfer (Hill et al., 2001; Tenneti et al., 2011). Thus, it always acts as a source of energy in homogeneous suspensions with a finite mean slip.

The covariance of gas-phase fluctuating velocities and divergence of stress tensor in Eq. B.2 is the dissipation of gas-phase velocity fluctuations. Using the chain rule, the dissipation can be written as

$$\left\langle u_i''^{(f)} \frac{\partial}{\partial x_j} \left(I^{(f)} \tau_{ji} \right) \right\rangle = \left\langle \frac{\partial}{\partial x_j} \left(u_i''^{(f)} I^{(f)} \tau_{ji} \right) \right\rangle - \left\langle I^{(f)} \tau_{ji} \frac{\partial u_i''^{(f)}}{\partial x_j} \right\rangle. \tag{B.9}$$

Commuting the averaging and gradient operators and applying statistical homogeneity assumption, the first term on the right-hand-side of the above equation will be zero. The gas-phase stress tensor $\boldsymbol{\tau}$ in the second term can be further dissected into pressure and viscous parts as

$$\tau_{ji} = -p\delta_{ij} + \mu^{(f)} \left(\frac{\partial u_i}{\partial x_j} + \frac{\partial u_i}{\partial x_j} \right). \tag{B.10}$$

Thus, the dissipation can be written as

$$\left\langle u_i''^{(f)} \frac{\partial}{\partial x_j} \left(I^{(f)} \tau_{ji} \right) \right\rangle = \underbrace{\left\langle I^{(f)} p \delta_{ij} \frac{\partial u_i''^{(f)}}{\partial x_j} \right\rangle}_{\Gamma} - \underbrace{\left\langle I^{(f)} \mu^{(f)} \left(\frac{\partial u_i''^{(f)}}{\partial x_j} + \frac{\partial u_j''^{(f)}}{\partial x_i} \right) \left(\frac{\partial u_i''^{(f)}}{\partial x_j} \right) \right\rangle}_{\Theta}. \tag{B.11}$$

This expression shows that the dissipation can be separated into pressure part Γ and viscous part Θ. Note that the presence of Kronecker delta in Γ invokes the continuity of the fluctuating velocity field. Thus, the pressure contribution to the dissipation is zero. The Θ term can further be simplified to obtain

$$\left\langle u_i''^{(f)} \frac{\partial}{\partial x_j} \left(I^{(f)} \tau_{ji} \right) \right\rangle = -2\mu^{(f)} \left\langle I^{(f)} s_{ij} s_{ij} \right\rangle, \tag{B.12}$$

where s_{ij} is the rate of strain tensor. Since the terms $\Pi^{(f)}$ and $\varepsilon^{(f)}$ are respectively described in Eqs. B.5 and B.12, the evolution equation of $k^{(f)}$ (Eq. B.2) can be rewritten as

$$(1-\phi)\rho^{(f)} \frac{\partial k^{(f)}}{\partial t} = \langle W_i \rangle \left\langle \tau_{ji} n_j^{(p)} \delta(\mathbf{x} - \mathbf{x}^{(I)}) \right\rangle - 2\mu^{(f)} \left\langle I^{(f)} s_{ij} s_{ij} \right\rangle. \tag{B.13}$$

Due to the importance viscous dissipation in the evolution of $k^{(f)}$, the convergence of $\varepsilon^{(f)}$ is studied in the next section.

B.2 Convergence test

The presence of particles in gas-solid flows changes the mechanism of gas-phase dissipation (Tenneti et al., 2012). This dissipation is no longer characterized by Kolmogorov scales, unlike single-phase turbulence. However, it is determined by high velocity gradients close to particle surface. Thus, it is useful to measure the dissipation at particle surfaces, particularly for modeling purposes.

Accurate measurement of gas-phase dissipation is very difficult, even in isotropic single-phase flows (Raffel et al., 2007). Direct measurement of dissipation from experiment is not possible. For instance, Hwang and Eaton (2006) used a LES analogy technique for dissipation measurement, assuming that the sub-grid scale energy flux from the integral scale to the Kolmogorov scale through the inertial sub-range is equal to the dissipation rate. On the other hand, computation of dissipation at particle surface from particle-resolved methods, such as PUReIBM, is not straightforward. Limited number of independent realizations causes high statistical errors (Xu and Subramaniam, 2010), since the sample space for surface measurable quantities is very small. Additionally, computation of dissipation in spherical coordinate from the solution data on a Cartesian coordinate is complicated. Since the sample space for volumetric measurable quantities is much larger than the surface measurable quantities, it is better to compute the volumetric dissipation in a region close to particle surface, called *near-particle* region. The volumetric dissipation depends on how far the near-particle region is extended above the particle surface. Accordingly, this region should contain the high velocity gradients generated in response to the interaction of the mean slip velocity with solid particles.

The importance of viscous dissipation in the evolution of $k^{(f)}$ necessitates the convergence test study of $\varepsilon^{(f)}$. In the following paragraphs, the convergence of viscous dissipation is presented for homogeneous gas-solid suspensions. The convergence of volumetric dissipation is studied for simple cubic configuration, and the near-particle volumetric dissipation is quantified for the random particle configurations considered in this work. Subsequently, quantification

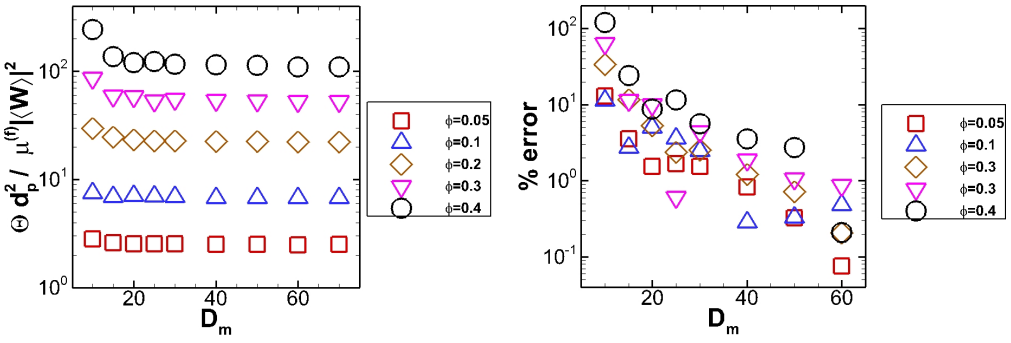

(a) (b)

Figure B.1 Convergence characteristics of dissipation for simple cubic configuration at $Re_m = 50$. Fig. B.1(a) shows normalized viscous dissipation, while Fig. B.1(b) shows Relative error of dissipation with respect to the case $D_m = 70$.

of viscous dissipation at particle surface with two methodologies is reported.

PR-DNS of simple cubic (SC) configuration is performed at $Re_m = 50$ (similar results observed for $Re_m = 20$; not represented here) with the range of particle resolution D_m 10–70, and solid volume fraction ϕ 0.05–0.4. Since in a statistically homogeneous system, ensemble-averaging can be estimated by volume-averaging, the viscous dissipation is computed as

$$\varepsilon^{(f)} = \frac{2\mu^{(f)}}{V^{(f)}} \int_{\mathcal{V}} I^{(f)} s_{ij} s_{ij} dV. \tag{B.14}$$

Quantification of $\varepsilon^{(f)}$ for the cases simulated (shown in Fig.B.1) clearly indicates the numerical convergence of volumetric dissipation with increasing grid resolution. Note that the strain rate tensor is computed by using the continuous stress field from the PUReIBM data, introducing error in the estimation of dissipation in cells adjacent to the particle surface (the stress field is not continuous in real suspensions). However, the volumetric dissipation is not affected due to the small ratio of volume occupied by these cells to the total volume of the gas phase.

According to Eq.B.12, viscous dissipation is significant in regions where the velocity gradient is considerable. In gas-solid suspensions, high velocity gradient regions form around particles due to the presence of a boundary layer. To identify the importance of near-particle dissipation, we used our PR-DNS data of random particle configurations to compute the ratio of near-particle dissipation to the total dissipation in the gas phase. The near-particle region is defined as a confined region between the particle surface and a sphere that is 5% greater in diameter

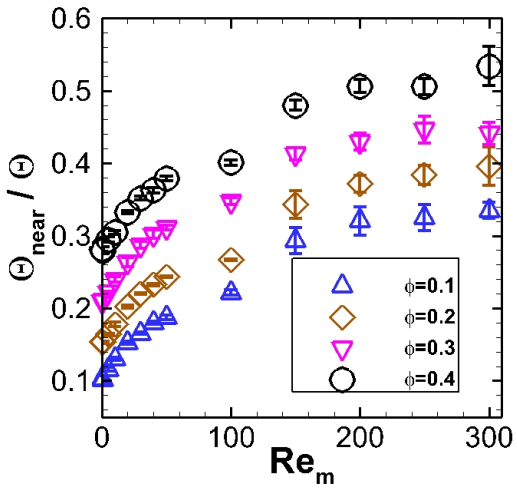

Figure B.2 The ratio of near-particle dissipation to the total viscous dissipation in the gas-phase for homogeneous particle assemblies.

than the particle. Fig. B.2 shows that near-particle dissipation is significant in gas-solid flows. This figure demonstrates that an increased ϕ results in an increased ratio for near-particle dissipation; the near-particle region volume increases compared to the total volume of the gas phase. In addition, an increase of the Reynolds number intensifies the magnitude of velocity gradients, causing the enhancement of dissipation. This finding motivates us to investigate the convergence of $\varepsilon^{(f)}$ at particle surface as well.

To compute the local dissipation at the particle surface, we use the definition of $\varepsilon^{(f)}$ given in Eq. B.2. Since the pressure contribution to the dissipation in a statistically homogeneous suspension is zero, we focus on the viscous contribution, that is

$$\varepsilon^{(f)}_{\text{local}} = u_i''^{(f)} \frac{\partial}{\partial x_j} \left(2\mu^{(f)} I^{(f)} s_{ji} \right). \tag{B.15}$$

In real gas-solid flows, the velocity field is continuous in the whole domain, while the stress tensor is discontinuous across the gas-solid interface. The presence of the indicator function in the above expression denotes the discontinuity of the stress field. However, in PUReIBM the stress tensor is continuous across the interface, as well as the velocity field. Thus, in order to compute the dissipation at a particle surface that is consistent with the mathematical formula, we neglect the velocity field inside particles and use only the gas-phase velocity field. Therefore,

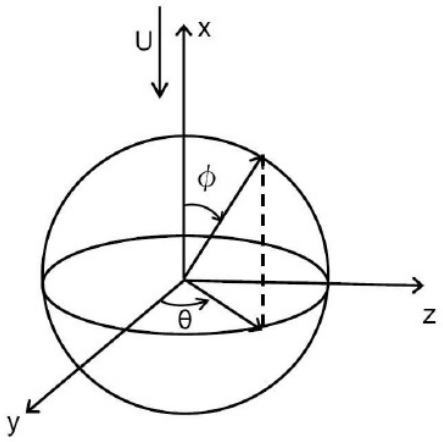

Figure B.3 The spherical coordinate system located at the center of particle.

the local dissipation is written as

$$\varepsilon_{\text{local}}^{(f)} = u_i''^{(f)} \frac{\partial}{\partial x_j} \left(2\mu^{(f)} s_{ji}^{(f)} \right), \tag{B.16}$$

the inner product of the gas-phase velocity fluctuations and the divergence of the gas-phase stress tensor. Additionally, quantification of dissipation at the particle surface requires transforming the velocity field from the Cartesian coordinate into a spherical coordinate, the origin of which is located at the particle center, as shown in Fig. B.3. Local viscous dissipation is then computed at the particle surface. Local viscous dissipation in spherical coordinate is written as

$$\varepsilon_{\text{local}}^{(f)} = \mu^{(f)} \left(u_r''^{(f)} (\nabla^2 \mathbf{U})_r + u_\theta''^{(f)} (\nabla^2 \mathbf{U})_\theta + u_\phi''^{(f)} (\nabla^2 \mathbf{U})_\phi \right). \tag{B.17}$$

The Laplacian of a vector in the spherical coordinate is defined as

$$\begin{aligned}
(\nabla^2 \mathbf{u})_r &= \nabla^2 u_r - \frac{2u_r}{r^2} - \frac{2}{r^2} \frac{\partial u_\theta}{\partial \theta} - \frac{2\cot\theta\, u_\theta}{r^2} - \frac{2}{r^2 \sin\theta} \frac{\partial u_\phi}{\partial \phi}, \\
(\nabla^2 \mathbf{u})_\theta &= \nabla^2 u_\theta + \frac{2}{r^2} \frac{\partial u_r}{\partial \theta} - \frac{u_\theta}{r^2 \sin^2\theta} - \frac{2\cot\theta}{r^2 \sin\theta} \frac{\partial u_\phi}{\partial \phi}, \\
(\nabla^2 \mathbf{u})_\phi &= \nabla^2 u_\phi - \frac{u_\phi}{r^2 \sin^2\theta} + \frac{2}{r^2 \sin\theta} \frac{\partial u_r}{\partial \phi} + \frac{2\cot\theta}{r^2 \sin\theta} \frac{\partial u_\theta}{\partial \phi},
\end{aligned} \tag{B.18}$$

with $\nabla^2 f$ being

$$\nabla^2 f = \frac{1}{r^2} \frac{\partial}{\partial r} \left(r^2 \frac{\partial f}{\partial r} \right) + \frac{1}{r^2 \sin\theta} \frac{\partial}{\partial \theta} \left(\sin\theta \frac{\partial f}{\partial \theta} \right) + \frac{1}{r^2 \sin^2\theta} \frac{\partial^2 f}{\partial \phi^2}. \tag{B.19}$$

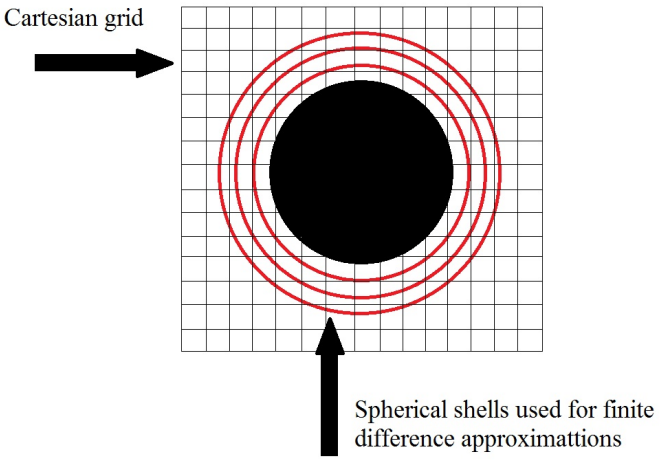

Figure B.4 Representation of spherical shells to compute one–sided derivatives for local viscous dissipation estimation

The local dissipation at particle surface is computed by quantification of these derivatives. Local dissipation is then averaged along the polar coordinate θ, that is perpendicular to the mean flow direction, and reported along the azimuthal coordinate ϕ, parallel to the flow direction. Two methods are employed to compute the derivatives in Eqs. B.18 and B.19 that are discussed bellow.

Finite difference approach

Gas-phase data is used to compute the derivatives by means of one–sided second order finite difference expressions, as shown in Fig. B.4. In this method, the velocity field is interpolated on spherical shell points. The local viscous dissipation computed from the gas-phase velocity field exhibits fluctuations as shown in Fig. B.5 for the case $\phi = 0.05$, $Re_m = 20$, and $D_m = 30$ as an example. There are two main reasons associated with this fluctuations:

1. PUReIBM employs a predictor-corrector method. The implementation of no-slip and no-penetration boundary conditions takes place in the predictor step. The corrector step, which ensures the continuity of the velocity field, does not guarantee that the boundary conditions are attained accurately.

2. In immersed boundary methods, the interpolation operator introduces a small numerical

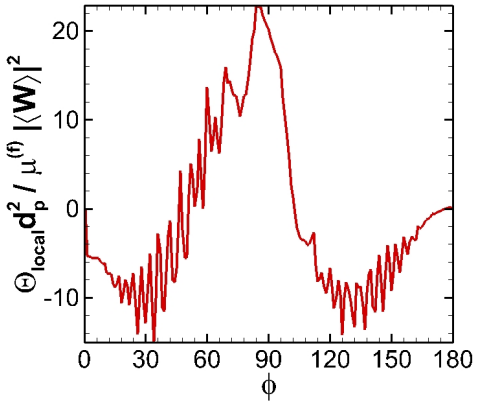

Figure B.5 Local viscous dissipation at particle surface for a SC configuration with $\phi = 0.05$, $Re_m = 20$, and $D_m = 30$, from the finite difference method

error into the field which is not removed through the solution.

These negligible errors co-exist near the gas-solid interface. Although they do not influence the flow quantities, they are reflected in the dissipation estimation when computation of higher order derivatives are required.

PHYSALIS method

Local viscous dissipation computed from the approach discussed above does not show convergence characteristics due to the presence of fluctuations. Consequently, we use another numerical method, called *PHYSALIS* (Prosperetti and Oguz, 2001), that produces a smooth analytical solution for velocity and pressure fields in the proximity of particles. This method assumes that very close to the particle surface the viscous forces are dominant, compared to inertial forces. Thus, the flow field can be represented by Stokes equations. An analytical Stokes flow is constructed by means of spherical harmonics, satisfying the no-slip and no-penetration boundary conditions at particle surfaces on one hand, and the inertial-dominant flow field from the Navier-Stokes solver on the other hand. The coupling between the Navier-Stokes solver and spherical harmonics takes place at *cage nodes*, the computational nodes being adjacent to the particle surface. In addition, the number of modes for the spherical harmonics should be determined. We use the PHYSALIS method with *four* modes in spherical harmonics to generate an analytical solution from our PR-DNS data to compute dissipation at the particle

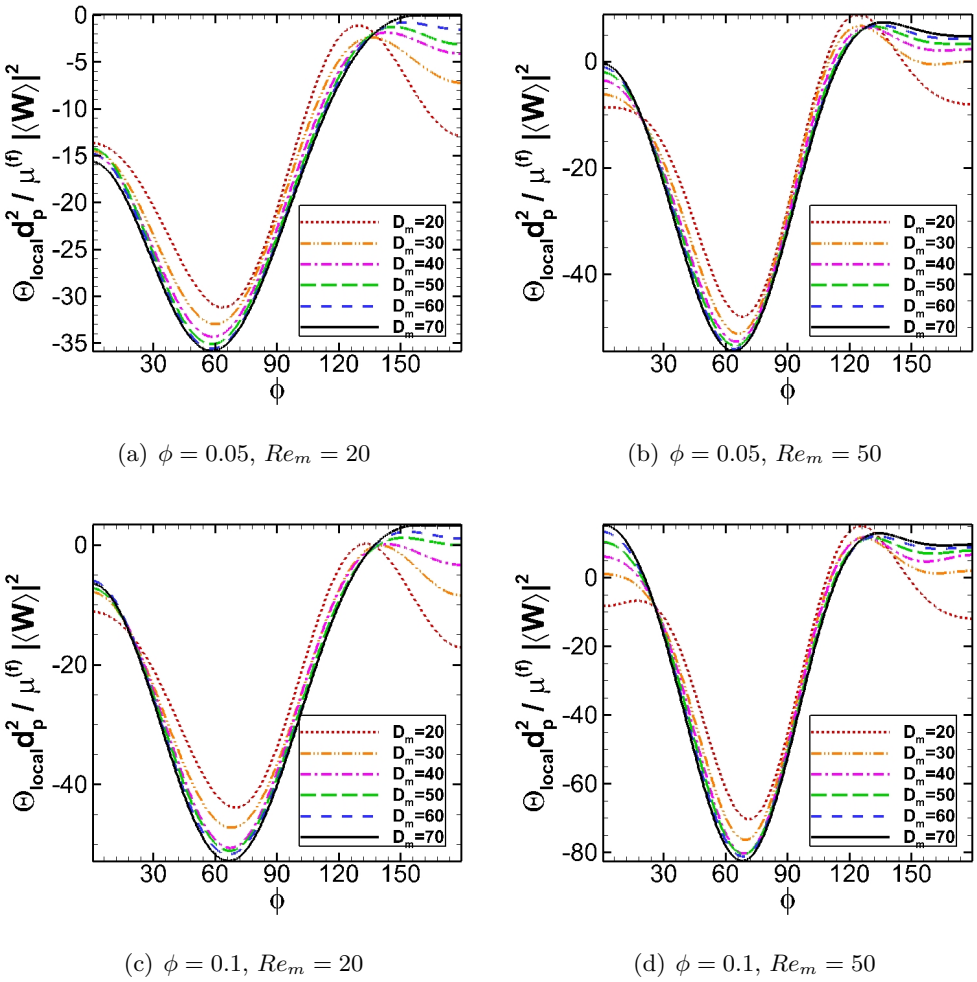

(a) $\phi = 0.05$, $Re_m = 20$

(b) $\phi = 0.05$, $Re_m = 50$

(c) $\phi = 0.1$, $Re_m = 20$

(d) $\phi = 0.1$, $Re_m = 50$

Figure B.6 Convergence characteristics of local viscous dissipation for simple cubic configuration, from the PHYSALIS method.

surface for SC configurations, as shown in Fig. B.6. Note that this method is only used for post-processing purposes, and is not coupled with the flow solver. The results indicate that the viscous dissipation exhibits convergence at particle surface with grid resolution for cases considered in this study. However, we should point out that the performance of PHYSALIS is strongly influenced by the number of modes in spherical harmonics. In addition, the validity of the method depends on the proximity of cage nodes to the particle surface for the validity of Stokes flow assumption. Moreover, the system of equations obtained by employing the boundary conditions on spherical harmonics is over-determined. A least square methodology is used to solve this system of equations, which gives an approximation to the exact solution. Thus,

even the smooth field from PHYSALIS cannot predict correctly the dissipation at particle surface.

Bibliography

Bagchi, P. and Balachandar, S. (2004). Response of the wake of an isolated particle to an isotropic turbulent flow. *Journal of Fluid Mechanics*, 518:95–123.

Balachandar, S. and Eaton, J. K. (2010). Turbulent dispersed multiphase flow. *Annual review of fluid mechanics*, 42:111–133.

Boivin, M., Simonin, O., and Squires, K. D. (1998). Direct numerical simulation of turbulence modulation by particles in isotropic turbulence. *J. Fluid Mech.*, 375:235–263.

Bolio, E. J., Yasuna, J. A., and Sinclair, J. L. (1995). Dilute turbulent gas-solid flow in risers with particle-particle interactions. *AIChE Journal*, 41(6):1375–1388.

Breault, R. W., Guenther, C. P., and Shadle, L. J. (2008). Velocity fluctuation interpretation in the near wall region of a dense riser. *Powder Technology*, 182(2):137 – 145.

Burton, T. M. and Eaton, J. K. (2005). Fully resolved simulations of particle-turbulence interaction. *Journal of Fluid Mechanics*, 545:67–111.

Chapman, S. and Cowling, T. G. (1953). *The mathematical theory of non–uniform gases.* Cambridge University Press, 2nd. edition.

Cocco, R., Shaffer, F., Hays, R., Karri, S. R., and Knowlton, T. (2010). Particle clusters in and above fluidized beds. *Powder Technology*, 203(1):3 – 11.

Cundall, P. A. and Strack, O. D. L. (1979). A discrete numerical model for granular assemblies. *Geotechnique*, 29:47–65.

Ding, J. and Gidaspow, D. (1990). A bubbling fluidization model using kinetic theory of granular flow. *AIChE Journal*, 36(4):523–538.

Doig, I. D. and Roper, G. H. (1967). Air velocity profiles in presence of cocurrently transported particles. *Industrial Engineering Chemistry Fundamentals*, 6(2):247–256.

Drew, D. A. (1983). Mathematical modeling of two–phase flow. *Annu. Rev. Fluid Mech.*, 15:261–291.

Drew, D. A. and Passman, S. L. (1998). *Theory of Multicomponent Fluids*. Applied Mathematical Sciences. Springer, New York.

Elghobashi, S. and Truesdell, G. C. (1993). On the two-way interaction between homogeneous turbulence and dispersed solid particles. i: Turbulence modification. *Physics of Fluids A: Fluid Dynamics*, 5(7):1790–1801.

Fan, R., Marchisio, D. L., and Fox, R. O. (2004). Application of the direct quadrature method of moments to polydisperse gas-solid fluidized beds. *Powder Technology*, 139(1):7 – 20.

Garg, R. (2009). *Modeling and simulation of two-phase flows*. PhD thesis, Iowa State University.

Garg, R., Galvin, J., Li, T., and Pannala, S. (2010). Documentation of open–source mfix–dem software for gas–solids flows. Technical report, National Energy Technology Laboratory, Department of Energy.

Garg, R., Tenneti, S., Mohd-Yusof, J., and Subramaniam, S. (2011). Direct numerical simulation of gas-solids flow based on the immersed boundary method. In *Computational Gas-Solids Flows and Reacting Systems: Theory, Methods and Practice*. IGI Global.

Halvorsen, B., Guenther, C., and O'Brien, T. J. (2003). CFD calculations for scaling of a bubbling fluidized bed . In *Proceedings of the AIChE annual meeting*, pages 16–21, San Francisco, CA. AIChE.

Hertz, P. (1909). Über den gegenseitigen durchschnittlichen Abstand von Punkten, die mit bekannter mittlerer Dichte im Raume angeordnet sind. *Mathematische Annalen*, 67:387–398.

Hill, R. J., Koch, D. L., and Ladd, A. J. C. (2001). Moderate–Reynolds–number flows in ordered and random arrays of spheres. *J. Fluid Mech.*, 448(243-278).

Hwang, W. and Eaton, J. K. (2006). Homogeneous and isotropic turbulence modulation by small heavy particles (St 50). *J. Fluid Mech.*, 564:361–393.

Johnson, A. A. and Tezduyar, T. E. (1997). 3D simulation of fluid-particle interactions with the number of particles reaching 100. *Computer Methods in Applied Mechanics and Engineering*, 145(3-4):301 – 321.

Kiger, K. T. and Pan, C. (2000). PIV technique for the simultaneous measurement of dilute two-phase flows. *Journal of Fluids Engineering*, 122(4):811–818.

Kim, J. and Moin, P. (1985). Application of a fractional-step method to incompressible Navier-Stokes equations. *Journal of Computational Physics*, 59:308–323.

Koch, D. L. (1990). Kinetic theory for a monodisperse gas–solid suspension. *Physics of Fluids*, A 2(10)(1711-1723).

Koch, D. L. and Sangani, A. S. (1999). Particle pressure and marginal stability limits for a homogeneous monodisperse gas–fluidized bed: kinetic theory and numerical simulations. *J. Fluid Mech.*, 400(229-263).

Lee, S. and Durst, F. (1982). On the motion of particles in turbulent duct flows. *International Journal of Multiphase Flow*, 8(2):125 – 146.

Louge, M. Y., Mastorakos, E., and Jenkins, J. T. (1991). The role of particle collisions in pneumatic transport. *Journal of Fluid Mechanics*, 231:345–359.

Moran, J. C. and Glicksman, L. R. (2003). Mean and fluctuating gas phase velocities inside a circulating fluidized bed. *Chemical Engineering Science*, 58(9):1867 – 1878.

Oakley, T. R., Loth, E., and Adrian, R. J. (1997). A two-phase cinematic PIV method for bubbly flows. *Journal of Fluids Engineering*, 119(3):707–712.

Pai, M. G. and Subramaniam, S. (2009). A comprehensive probability density function formalism for multiphase flows. *Journal of Fluid Mechanics*, 628:181–228.

Peskin, C. S. (2002). The immersed boundary method. *Acta Numerica*, 11:479–517.

Pita, J. A. and Sundaresan, S. (1993). Developing flow of a gas-particle mixture in a vertical riser. *AIChE Journal*, 39(4):541–552.

Pope, S. B. (2000). *Turbulent Flows*. Cambridge University Press, Port Chester, NY.

Prosperetti, A. and Oguz, H. (2001). Physalis: A new o(N) method for the numerical simulation of disperse systems: Potential flow of spheres. *Journal of Computational Physics*, 167(1):196–216.

Pruppacher, H. R., Le Clair, B. P., and Hamielec, A. E. (1970). Some relations between drag and flow pattern of viscous flow past a sphere and a cylinder at low and intermediate Reynolds numbers. *Journal of Fluid Mechanics*, 44(4):781–790.

Raffel, M., Willert, C., Wereley, S., and Kompenhans, J. (2007). *Particle image velocimetry: A practical Guide*. Springer, 2nd. edition.

Rogallo, R. S. (1981). Numerical experiments in homogeneous turbulence. *Nasa Technical Report*, (81835).

Rogers, C. B. and Eaton, J. K. (1991). The effect of small particles on fluid turbulence in a flat plate, turbulent boundary layer in air. *Physics of Fluids*, 3(5):928–937.

Sangani, A. S., Mo, G., Tsao, H.-K. W., and Koch, D. L. (1996). Simple shear flows of dense gas–solid suspensions at finite Stokes numbers. *J. Fluid Mech.*, 313(309-341).

Sato, Y., Hishida, K., and Maeda, M. (1996). Effect of dispersed phase on modification of turbulent flow in a wall jet. *Journal of Fluids Engineering*, 118(2):307–315.

Simonin, O. (1996). Continuum modeling of dispersed turbulent two-phase flows: Combustion and turbulence in two-phase flows. *von Kármán Institute of Fluid Dynamics Lecture Series*.

Sinclair, J. L. and Jackson, R. (1989). Gas-particle flow in a vertical pipe with particle-particle interactions. *AIChE Journal*, 35(9):1473–1486.

Speight, J. G. (2006). *The chemistry and technology of petroleum*. CRC Press, 4th. edition.

Squires, K. D. and Eaton, J. K. (1990). Particle response and turbulence modification in isotropic turbulence. *Phys. Fluids A*, 2:1191–1203.

Stoyan, D., Kendall, W. S., and Mecke, J. (1995). *Stochastic Geometry and its Applications*. Wiley Series in Probability and Mathematical Statistics. John Wiley and Sons, New York, 2nd edition.

Sun, J., Battaglia, F., and Subramaniam, S. (2007). Hybrid two-fluid DEM simulation of gas-solid fluidized beds. *Journal of Fluid Engineering*, 129(11):1394–1403.

Sundaram, S. and Collins, L. R. (1999). A numerical study of the modulation of isotropic turbulence by suspended particles. *J. Fluid Mech.*, 379:105–143.

Tenneti, S., Garg, R., Hrenya, C., Fox, R., and Subramaniam, S. (2010). Direct numerical simulation of gas-solid suspensions at moderate Reynolds number: Quantifying the coupling between hydrodynamic forces and particle velocity fluctuations. *Powder Technology*, 203(1):57 – 69.

Tenneti, S., Garg, R., and Subramaniam, S. (2011). Drag law for monodisperse gas-solid systems using particle-resolved direct numerical simulation of flow past fixed assemblies of spheres. *International Journal of Multiphase Flow*, 37(9):1072 – 1092.

Tenneti, S., Garg, R., and Subramaniam, S. (2012). Fluid-phase velocity fluctuations in statistically homogeneous gas-solid flow using particle-resolved direct numerical simulation. Part ii: Freely evolving suspensions. (Submitted to IJMF).

Torquato, S., Lu, B., and Rubinstein, J. (1990). Nearest-neighbor distribution functions in many-body systems. *Phys. Rev. A*, 41:2059–2075.

Uhlmann, M. (2008). Interface-resolved direct numerical simulation of vertical particulate channel flow in the turbulent regime. *Physics of Fluids*, 20(5):053305.

van der Hoef, M. A., Beetstra, R., and Kuipers, J. A. M. (2005). Lattice-Boltzmann simulations of low-Reynolds-number flow past mono- and bidisperse arrays of sphere: results for the permeability and drag force. *Journal of Fluid Mechanics*, 528:233–254.

Wylie, J. J., Koch, D. L., and Ladd, A. J. (2003). Rheology of suspensions with high particle inertia and moderate fluid inertia. *Journal of Fluid Mechanics*, 480:95 – 118.

Xu, Y. and Subramaniam, S. (2006). A multiscale model for dilute turbulent gas-particle flows based on the equilibration of energy concept. *Physics of Fluids*, 18(3):033301.

Xu, Y. and Subramaniam, S. (2007). Consistent modeling of interphase turbulent kinetic energy transfer in particle-laden turbulent flows. *Physics of Fluids*, 19(8):085101.

Xu, Y. and Subramaniam, S. (2010). Effect of particle clusters on carrier flow turbulence: A direct numerical simulation study. *Flow, Turbulence and Combustion*, 85:735–761.

Yin, X. and Koch, D. L. (2007). Hindered settling velocity and microstructure in suspensions of spheres with moderate Reynolds number. *Physics of Fluids*, 19:093302.

Yusof, J. M. (1996). *Interaction of Massive Particles with Turbulence*. PhD thesis, Cornell University.

Zhang, Z. and Prosperetti, A. (2005). A second-order method for three-dimensional particle simulation. *Journal of Computational Physics*, 210(1):292 – 324.

Zick, A. A. and Homsy, G. M. (1982). Stokes flow through periodic arrays of spheres. *J. Fluid Mech.*, 115:13–26.